Mon. Not. R. Astron. Soc. **000**, 1–?? (2007) Printed 23 August 2016 (MN LATEX style file v2.2)

Low-mass disc galaxies and the issue of stability: MOND vs dark matter

arXiv:1608.06264v1 [astro-ph.GA] 22 Aug 2016

F. J. Sánchez-Salcedo[1⋆], E. Martínez-Gómez[2], V. M. Aguirre-Torres[2] and H. M. Hernández-Toledo[1]

[1]*Instituto de Astronomía, Universidad Nacional Autónoma de México, Ciudad Universitaria, Apt. Postal 70 264, C.P. 04510, Mexico City, Mexico*

[2]*Departamento de Estadística, Instituto Tecnológico Autónomo de México (ITAM), Rio Hondo 1, C.P. 01080, Mexico City, Mexico*

Accepted xxxx Month xx. Received xxxx Month xx; in original form 2016 April 12

ABSTRACT

We analyse the rotation curves and gravitational stability of a sample of six bulgeless galaxies for which detailed images reveal no evidence for strong bars. We explore two scenarios: Newtonian dark matter models and MOdified Newtonian Dynamics (MOND). By adjusting the stellar mass-to-light ratio, dark matter models can match simultaneously both the rotation curve and bar-stability requirements in these galaxies. To be consistent with stability constraints, in two of these galaxies, the stellar mass-to-light ratio is a factor of $\sim 1.5-2$ lower than the values suggested from galaxy colours. In contrast, MOND fits to the rotation curves are poor in three galaxies, perhaps because the gas tracer contains noncircular motions. The bar stability analysis provides a new observational test to MOND. We find that most of the galaxies under study require abnormally-high levels of random stellar motions to be bar stable in MOND. In particular, for the only galaxy in the sample for which the line-of-sight stellar velocity dispersion has been measured (NGC 6503), the observed velocity dispersion is not consistent with MOND predictions because it is far below the required value to guarantee bar stability. Precise measurements of mass-weighted velocity dispersions in (unbarred and bulgeless) spiral galaxies are crucial to test the consistency of MOND.

Key words: galaxies: kinematics and dynamics – dark matter – gravitation – methods: statistical

1 INTRODUCTION

The rotation curves of spiral galaxies are very useful to measure the mass distribution in these objects. The discrepancy between the dynamical mass and the luminous mass is considered as a strong evidence of the existence of dark matter in these galaxies. Alternatively, the mass discrepancy can be interpreted as a breakdown of the Newtonian law of gravity. In particular, MOdified Newtonian Dynamics (MOND), in which the gravitational force is larger than the standard Newtonian gravitational force at accelerations below a value $a_0 \sim 1.2\times10^{-8}$ cm s^{-2}, can account for the shape and amplitude of the rotation curves of spiral galaxies amazingly well, except for a handful of galaxies (e.g., Sanders & McGaugh 2002; Bottema et al. 2002; Milgrom & Sanders 2007; Sanders & Noordermeer 2007; Swaters et al. 2010; Gentile et al. 2011; Sánchez-Salcedo et al. 2013; Randriamampandry & Carignan 2014; Rodrigues et al. 2014; Bottema & Pestaña 2015) In practice, the quality of MOND fits to the rotation curves are sensitive to uncertainties in the adopted parameters of the galaxy such as inclination, distance or the adopted form of the interpolating function $\mu(x)$. In addition, noncircular motions and warps may also affect the observed rotation curve. Thus, it is important to investigate other gravitational effects which can offer independent tests (see Sanders & McGaugh 2002; Famaey & McGaugh 2012, for a compilation of evidence that supports MOND).

In the dark matter models, the separate contributions to the rotation curve from the baryonic components and dark matter are not easily disentangled because equally well-fitting models to the rotation curve can be obtained with different stellar mass-to-light ratios. For unbarred galaxies, disc stability constraints may provide upper limits on the surface density of stellar discs or, equivalently, to the stellar mass-to-light ratio $\Upsilon_\star$ (Athanassoula et al. 1987; Fuchs & von Linden 1998; Fuchs 2008; Lisker & Fuchs 2009; Puglielli et al. 2010; D'Onghia 2015).

It is usually argued that unbarred galaxies with slowly rising rotation curves at the centre are stabilized against bar instabilities by dark haloes, whereas unbarred galaxies with circular velocities $\gtrsim 150$ km s^{-1} use to present a steep inner rise in the rotation curve and may be stabilized by their hard centres (e.g., Sellwood & Evans 2001). In the case of dwarf galaxies and low-surface brightness (LSB) galaxies, many studies led to the generally accepted pic-

⋆ E-mail:jsanchez@astro.unam.mx

© 2007 RAS

ture that many of these galaxies are dominated by dark matter at almost all radii, especially those galaxies that have gently rising rotation curves (e.g., Carignan & Freeman 1988; Persic et al. 1996; Côté et al. 2000; de Blok et al. 2001; Swaters et al. 2011) For instance, Swaters et al. (2011) considered a sample of 18 ealy-type dwarf galaxies and found that if the stellar mass-to-light ratio in the R-band is assumed to be near unity, as predicted by stellar population synthesis, all galaxies except one are dominated by dark matter. The dominant dark matter halo and the low surface density could explain the rarity of bars in LSB galaxies (Mihos et al. 1997). Still, some LSB galaxies may be massive enough to become bar unstable (Mayer & Wadsley 2004). Rotating haloes, triaxial haloes, the dynamical state of cosmological haloes, the physics of gas and baryons, and tidal interactions may lead to bar formation even in some dwarf and LSB galaxies (Weinberg & Katz 2002; Curir et al. 2006; Saha & Naab 2013; Ghosh et al. 2016). Due to all these factors, predictions on the fraction of barred galaxies as a function of Hubble type are difficult.

In MOND, the rotation curve sets the mass-to-light ratio of the stellar disc and thus there is less freedom to adjust the surface density of the disc, which is a crucial determinant in the stability analysis. Although it is simple to show from the basic tenets of MOND, that discs with low internal accelerations (deep MOND regime) are more stable than purely Newtonian discs (Milgrom 2014), the added stability is limited. Indeed, discs in the deep MOND regime are more unstable in MOND than in the equivalent Newtonian galaxy, that is the same disc but embedded in a rigid halo to have the same circular velocity. Given the limited stability provided by MOND, the following questions arise: does MOND predict the correct level of stability in galaxies with gently rising rotation curves at their centres? What about the stability of galaxies that are not in the deep MOND regime? McGaugh & de Blok (1998) and Famaey & McGaugh (2012) argued that MOND naturally provides the required level of disc self-gravity to explain the existence of bars and spiral structure observed in some (red) LSB galaxies (although the spiral arms in these galaxies are fragmentary, extremely faint and difficult to trace).

Stability studies in pressure-supported stellar systems can be also used to discriminate between modified gravity theories and Newtonian gravity plus a dark matter halo. Nipoti, Ciotti & Londrillo (2011) found that MOND systems are more prone to radial-orbit instability than their equivalent Newtonian systems. They suggested that stability constraints combined with their measured velocity dispersion profiles in globular clusters (e.g., NGC 2419) and dwarf spheroidal galaxies could provide crucial tests for MOND models.

In this work, we have selected six pure-disc galaxies having high-quality rotation curves in their inner regions. We consider separately the standard dark matter scenario and MOND. To be satisfactory, the models should be able to reproduce correctly the shape and amplitude of the rotation curves for reasonable values of $\Upsilon_\star$, but also the level of gravitational stability of the disc in these galaxies. Since the selected galaxies do not have a dense centre able to stabilize the stellar disc against bar-forming modes, high levels of instability would be very difficult to reconcile with detailed images that reveal no evidence for the presence of strong bars. Moreover, if MOND is a good effective theory (albeit not definitive) to describe the phenomenology of galaxies, the stability analysis in the MOND framework may be used as a tool to make testable predictions.

The paper is organised as follows. In Section 2 we present the theoretical basis and the disc-stability criteria in Newtonian dynamics and in MOND. In Section 3 we briefly describe the properties of the selected galaxies. Section 4 presents the fits to the rotation curves and the stability analysis under the standard dark matter scenario. In Section 5, we perform the same analysis but in the MOND framework. Final comments and conclusions can be found in Section 6. A statistical Appendix is provided to describe the Bayesian approach used to draw inferences on the relevant parameters and functions of these parameters.

2 STABILITY CONSTRAINTS: THEORETICAL FRAMEWORK

2.1 Newtonian dynamics

There is a solid embodiement to suggest that the multicomponent (cold gas, warm gas and stars) Toomre stability parameter Q lies in the range $1 < Q < 2.5$ within the optical radius of disc galaxies. The Toomre parameter is required to be > 1 to avoid a violent fragmentation instability but it is generally less than 2.5 in order to allow the discs to have a level of self-gravity enough to develop spiral structures and self-regulated star formation (Sellwood & Carlberg 1984; Athanassoula & Sellwood 1986; Bottema 1993, 2003; Fuchs 1999, 2001, 2008; Khoperskov et al. 2003; Zasov et al. 2004; Roskar et al. 2012; Romeo & Falstad 2013; Forbes et al. 2014).

2.1.1 Spiral arms and the X_m-parameter

In cold discs (i.e. $1 < Q < 2.5$), swing amplification of perturbations in the disc may lead to the grow of non-axisymmetric structures (Toomre 1981). For a disc with surface density Σ and epicyclic frequency κ, the wavelength that preferently grows, $\lambda_{\rm max}$, can be written as $\alpha\lambda_{\rm crit}$ where

$$\lambda_{\rm crit} = \frac{4\pi^2 G\Sigma}{\kappa^2}, \tag{1}$$

and α is a dimensionless factor which depends on the local derivative of the circular velocity. For instance, if the rotation curve is parameterized by a power-law, $v_c \propto R^\beta$, then $\alpha \simeq 2$ when $\beta = 0$ (flat rotation curve), and $\alpha \simeq 1.25$ when $\beta = 0.4$ (Athanassoula 1984; Fuchs 2001; Mayer et al. 2001). For linearly rising rotation curves ($\beta \simeq 1$), the low rate of differential rotation suppresses the swing amplification. However, resonances may support global modes (Lynden-Bell 1979) and the spiral structure is difficult to predict.

The density wave theory predicts that the number of spiral arms or multiplicity m is given by

$$m(R) = \frac{2\pi R}{\alpha\lambda_{\rm crit}} = \frac{R\kappa^2}{2\pi G\alpha\Sigma}. \tag{2}$$

It is convenient to define the X_m-parameter, which depends on R, as

$$X_m(R) = \frac{R\kappa^2}{2\pi G m\Sigma}. \tag{3}$$

The maximum amplification of the mode with multiplicity m will occur at those radii for which $X_m \simeq \alpha$ (Toomre 1981; Athanassoula 1984; Athanassoula et al. 1987; Fuchs 2001; D'Onghia 2015). According to Equation (3), discs of a fixed rotation curve should exhibit higher spiral-arm multiplicity (and a smaller amplitude of the arms) when the disc mass is decreased. Combining Eqs. (2) and (3), it is simple to show that the predicted number of arms can be determined from X_2 through the relation $m(R) = 2\alpha^{-1}X_2$.

The spiral arm multiplicity has been used as a powerful tool to constrain the mass of the disc in spiral galaxies and, thereby, the stellar mass-to-light ratio (Athanassoula et al. 1987; Fuchs & von Linden 1998; Fuchs 1999, 2008; Puglielli et al. 2010; Puglielli 2011; D'Onghia 2015). The analysis above is valid under the assumption that the stellar discs are dynamically cold (i.e. $Q \lesssim 2.2 - 2.5$). In hot discs, however, the amplification factor due to the swing amplification may be highly suppressed (Toomre 1981; Athanassoula 1984; Fuchs 2001; Ghosh & Jog 2014). Still, galaxies may present occasional, weak spiral structures due to resonances (Ghosh & Jog 2014) or interactions with companions.

2.1.2 *Bar-instability criteria*

If galactic discs are cold and massive, they may generate a large bar structure. As a diagnostic of the expected morphology of a certain galaxy, it would be very useful to have a recipe to predict when galaxies develop $m = 2$ spiral arms or form a bar. Although X_2 might be used as a diagnostic for bar formation (e.g., Mihos et al. 1997), it was derived in linear theory and strictly it cannot provide a criterion to distinguish bar stable to bar unstable discs. One has to use numerical simulations to study collective global instabilities.

Efstathiou, Lake & Negroponte (1982, hereafter ENL) derived a stability criterion for bar formation in isolated (bulgeless) galaxies; cold exponential discs with a Toomre parameter close to but larger than 1 are bar stable if

$$\mathcal{R} \equiv \frac{v_{\rm max}}{(GM_d/h_R)^{1/2}} > 1.1, \tag{4}$$

where $v_{\rm max}$ is the maximum rotational velocity, M_d is the mass of the disc and h_R its radial scale length. The ENL criterion provides an approximate indicator for stability in cold galaxies ($1 < Q < 2$) lacking a dense core or bulge (Mayer & Wadsley 2004; Yurin & Springel 2015; Barnes 2016). Once $v_{\rm max}$ and h_R are measured, this criterion sets an upper value on M_d and thereby on $\Upsilon_\star$, which we denote by $\Upsilon_\star^{\rm (ENL)}$. It is important to note that the ENL criterion was derived for discs in rigid haloes[1]. If haloes are made of collisionless particles, the disc-halo interaction produces a destabilizing influence (Athanassoula 2008; Sellwood 2016), which may lead to the formation of bars in galaxies that are bar stable by the ENL criterion. Thus, in bulgeless galaxies the $\Upsilon_\star^{\rm (ENL)}$ values should be considered as conservative upper limits, unless the level of random stellar motions are larger than usually assumed in these simulations.

Puglielli et al. (2010, hereafter PWC) found that a strong bar is formed if two conditions are met. The first one is that the minimum value of Q along the disc, denoted by $Q_{\rm min}$, is less than 2.2. The second condition is that $\langle X_2 \rangle < 2.7$, where the brakets $\langle ... \rangle$ represent the average value over two radial scale-lengths (see also Puglielli 2011), but excluding the central region $R < 2h_z$ (h_z the vertical scaleheight, which is assumed to be one fifth of the radial scalelength), where the razor-thin disc approximation is not valid. This condition imposes a maximum value for the stellar mass-to-light ratio, $\Upsilon_\star^{\rm (PWC)}$, for galaxies with no strong bars.

2.2 MOND

We will consider MOND as a modification of gravity's law, rather than a change in the inertia. We consider two popular 'modified-gravity' formulations of MOND, which provide a field equation between the density distribution of a system ρ and its associated gravitational potential Φ. The first one is the non-linear extension of the Poisson equation suggested by Bekenstein & Milgrom (1984) given by

$$\boldsymbol{\nabla} \cdot \left[\mu \left(\frac{|\boldsymbol{\nabla}\Phi|}{a_0} \right) \boldsymbol{\nabla}\Phi \right] = 4\pi G\rho, \tag{5}$$

where a_0 is a universal acceleration of the order of 10^{-8} cm s^{-2}, and $\mu(x)$ is some interpolating function with the property that $\mu(x) = x$ for $x \ll 1$ and $\mu(x) = 1$ for $x \gg 1$. The interpolating function may have different forms. A family of μ-functions that satisfies the required asymptotes are

$$\mu(x) = \frac{x}{(1+x^n)^{1/n}} \tag{6}$$

(Milgrom & Sanders 2008). The case $n = 2$ corresponds to the standard form proposed by Milgrom (1983), whereas the case $n = 1$ is the so-called "simple" μ-function suggested by Famaey & Binney (2005).

The second one is the quasi-linear MOND (QUMOND) formulation developed by Milgrom (2010):

$$\nabla^2\Phi = \boldsymbol{\nabla} \cdot \left[\nu \left(\frac{|\boldsymbol{\nabla}\Phi_N|}{a_0} \right) \boldsymbol{\nabla}\Phi_N \right], \tag{7}$$

where Φ_N is the Newtonian potential, which satisfies the standard Poisson equation $\nabla^2\Phi_N = 4\pi G\rho$. The non-linear modified Poisson equation and QUMOND are equivalent in a spherical distribution of mass if $\nu(y) = 1/\mu(x)$, where $y = x\mu(x)$.

2.2.1 *The X_m parameter in MOND*

Using the non-linear Poisson equation (Eq. 5), Milgrom (1989) found that the perturbations in MOND behave as in Newtonian dynamics but replacing the Newton constant G by $\chi_{nl}G$, with $\chi_{nl} = 1/[\mu^+(1+L^+)^{1/2}]$, where $L = d\ln\mu/d\ln x$, and μ^+ and L^+ are the values of μ and L, just above the disc. To obtain this result, he used the standard WKB approximation, where the disc has negligible thickness and the perturbations are tighly wound. Therefore, the Toomre and X_m parameters in the non-linear extension of the Poisson equation are

$$Q_M = \mu^+(1+L^+)^{1/2}\frac{\sigma_R\kappa}{3.36G\Sigma}, \tag{8}$$

and

$$X_m(R) = \mu^+(1+L^+)^{1/2}\frac{R\kappa^2}{2\pi Gm\Sigma}, \tag{9}$$

where σ_R is the radial velocity dispersion.

The prefactor $\mu^+(1+L^+)^{1/2}$ is in general ≤ 1. Consequently, MOND discs should exhibit a lower spiral-arm multiplicity and a larger amplitude of the arms than their equivalent Newtonian systems. In the Newtonian regime, it holds that $L^+ = 0$ and $\mu^+ = 1$, and hence the prefactor is equal to 1. In the deep MOND regime, $L^+ \to 1$ and thus the prefactor is $\simeq \sqrt{2}\mu^+$. However, it is misleading to think that galaxies in the deep MOND regime (i.e., galaxies with $\mu^+ \ll 1$) will have very small X_m-values. Indeed, κ depends on μ because of the boost that MOND produces in the rotation velocity. In Appendix A, we calculate X_m in terms of Newtonian quantities. We show that a MOND galaxy has the same X_m as a Newtonian galaxy with a nonresponsive dark halo whose mass is twice the mass of the disc, at most. In galaxies with internal accelerations $\gtrsim a_0$, the added stability in MOND is more limited; the

[1] There do exist dark matter candidates that behave more rigidly than a collisionless fluid (e.g., scalar field dark matter, see Slepian & Goodman 2012).

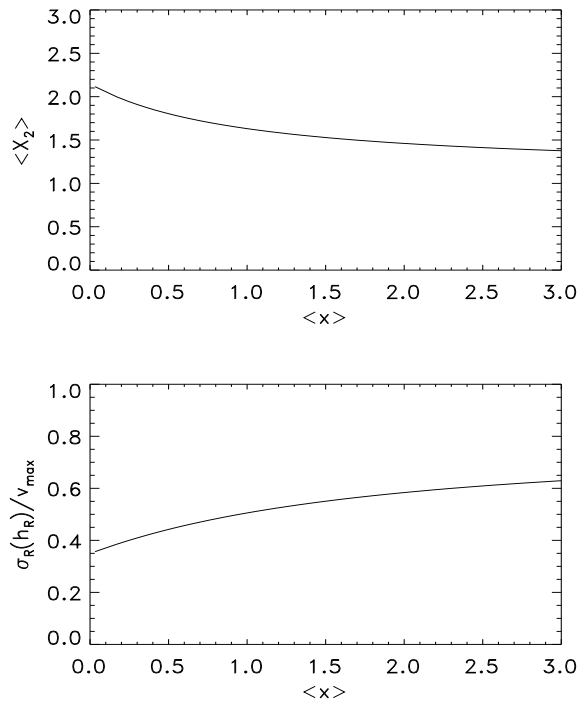

Figure 1. $\langle X_2 \rangle$ (top panel) and the ratio $\sigma_R/v_{\rm max}$ (with σ_R evaluated at one radial scale length h_R) to have $Q_M = 2.2$ (bottom panel), as a function of the mean internal acceleration (in units of a_0). We have assumed a very thin exponential disc and used the simple interpolating function.

same X_m parameter can be achieved in a Newtonian disc by adding an inert dark halo having a mass less than half the mass of the disc.

In general, the level of stability in MOND comes from the basic tenets of the MOND theory (Milgrom 2014) and thus it is expected to depend only slightly on the formulation. In Appendix B, we present the derivation of the X_m-parameter in the QUMOND formulation. It turns out that the Toomre parameter and the X_m-parameter in QUMOND are slightly smaller than the values using the non-linear Poisson equation. In the remainder of the paper, for definiteness, we adopt for X_2 the expression derived using the non-linear Poisson equation.

2.2.2 Bar-instability criteria in MOND

According to Equation (8), $Q_M \leq Q_{N,eq}$, where $Q_{N,eq}$ is the Toomre parameter in the equivalent Newtonian + halo system (that is, a halo is added to have the same circular velocity). Therefore, galaxies in MOND are expected to be more unstable, locally and globally, than their equivalent Newtonian galaxies. Brada & Milgrom (1999) tested numerically that the growth rate of the $m = 2$ Fourier mode is larger (or equal) in MOND discs than it is in the equivalent Newtonian disc + halo system. The formation and evolution of a bar in MOND and in Newtonian dynamics were described in Tiret & Combes (2007). They found that the bars in MOND galaxies develop very soon as compared to the Newtonian dark matter models. Since MOND discs are more unstable than their Newtonian dark matter analogs, discs with $\mathcal{R} < 1.1$ are also expected to be bar unstable in MOND. In fact, the ENL criterion does not take into account the enhanced self-gravity of the disc in MOND.

The PWC criterion for the formation of bars may be more restrictive than the ENL criterion. To illustrate this, consider a pure-stellar disc having a negligible thickness and a surface density following an exponential profile. Figure 1 shows $\langle X_2 \rangle$ as a function of $\langle x \rangle$ (where $x = |\boldsymbol{\nabla}\Phi|/a_0$ was taken at the midplane of the disc) for the simple μ-function. Bare Newtonian discs have $\langle x \rangle \gg 1$, $\langle X_2 \rangle = 1.15$, and are very unstable to bars. When we move from bare Newtonian discs to MOND discs, $\langle X_2 \rangle$ increases but only slightly; $\langle X_2 \rangle$ is not larger than 2.1 even for galaxies in the deep MOND regime ($\langle x \rangle \ll 1$). Indeed, it is not possible in MOND to satisfy the condition $\langle X_2 \rangle > 2.7$. This is a consequence of the limited stability of MOND discs already discussed in Milgrom (1989) and Brada & Milgrom (1999). In other words, if galaxies have cold discs and do not contain hard cores, disc self-gravity in MOND is strong enough to form bars, no matter how low the surface density of the disc is. In order for galaxies with $\langle X_2 \rangle \leq 2$, as predicted in the MOND framework, to be bar stable, they need to be dynamically hot. This may be accomplished if the Toomre parameter is above some threshold value ~ 2.2 (e.g., Athanassoula & Sellwood 1986). The condition $Q_M = 2.2$ provides a lower limit to the radial velocity dispersion σ_R. Figure 1 also shows the ratio between the radial velocity dispersion at one scale length (h_R) and the maximum rotational velocity in order to match the condition $Q_M = 2.2$ in a thin exponential disc. We see that discs with $\langle x \rangle \gtrsim 1$ require $\sigma_R(h_R) > 0.5 v_{\rm max}$ to be bar stable. Some questions arise: are unbarred galaxies (having no central hard cores) stable against bars because the stellar discs have high velocity dispersions? If the stellar discs were dynamically heated by a bar which was finally dissolved, why do not all the galaxies have a prominent bulge? The other less appealing possibility is that unbarred galaxies contain a stabilizing (unseen) spheroidal mass component, or a nonresponsive (unseen) thick disc, even in MOND. In order to shed light on these issues and to illustrate how unbarred galaxies can be used to test modified gravity theories, we have analysed a sample of bulgeless galaxies showing no strong evidence for bars.

3 THE SAMPLE OF GALAXIES: PHOTOMETRIC AND KINEMATICAL DATA

In the last decades, a great effort has been made to obtain high-quality rotation curves in the central regions of LSB galaxies and dwarf irregular galaxies to test the predictions of the standard cold dark matter model and the possible role of the baryonic feedback in shaping the central density profiles of dark haloes. Here, we analyse the dynamics of one Sd galaxy and five low-luminosity Sc galaxies, having high-resolution rotation curves in the inner regions: NGC 3621, 4605, 5949, 5963, 6503 and 6689. All the galaxies are nearby ($D < 15$ Mpc). Table 1 summarizes the basic parameters of these galaxies. The photometric inclinations of these galaxies vary between 48.4° for NGC 5963 to 76.0° for NGC 6689.

Combined three-band optical images, Spitzer IRAC images at 3.6 microns and subtracted-continuum Hα images are displayed in Figures 2 and 3. In order to assess the morphology of these galaxies, free from the effect of projection, the 3.6μm and Hα images were deprojected. To deproject each galaxy, flux-conserving stretching perpendicular to the line of nodes was carried out by using IRAF routines and by assuming that the outer disc should be intrinsically circular. Major axis position angles (North Eastwards), axis ratios (the major-to-minor axis ratio up to the 25 mag arcsec^{-2} isophote in the B-band) and inclinations between the line of sight and the polar axis were all taken from HyperLeda database

Table 1. Comparison of the relevant parameters of the selected galaxies and references

Name	D (Mpc)	M_B	μ_0 (mag arcsec^{-2})	i (deg)	$2h_R$ (kpc)	References for parameters	References and databases for Figs 2-3
NGC 3621	6.64 ± 0.50	-20.05	18.2	$66°$	3.3	F01, dB08, G11	SING
NGC 4605	4.26± 0.64	-17.7	21.0	$71.5°$	1.36	S05	SDSS-DR7, D09
NGC 5949	14.0 ± 2.4	-18.2	21.2	$64.6°$	3.0	S05	SDSS-DR7, D09
NGC 5963	13 ± 3	-17.8	20.1	$48.4°$	1.36	S05	SDSS-DR7, S10, J04
NGC 6503	5.2 ± 1	-17.7	19.2	$74°$	2.8	K97, M99, B87	L07, S10, D09
NGC 6689	11	-17.6	20.8	$76.0°$	2.3	S05	T05, SEIP, J04

Column (1): Name of the galaxy. Column (2): Distance. Column (3): Absolute B magnitude. Column (4): Extrapolated central surface brightness in the B-band, except for NGC 6689, which is in the V-band. Column (5): Photometric inclination. Column (6): $2h_R$ is the distance at which the stellar surface density drops a factor of $\exp(2)$ from its central value. Column (7): References for the parameters (F01: Freedman et al. 2001; dB08: de Blok et al. 2008; G11: Gentile et al. 2011; S05: Simon et al. 2005; K97: Karanchentsev & Sharina 1997; M99: Makarova 1999; B87: Begeman 1987). Column (8): References of the optical, infrared and continuum-subtracted Hα images (SING: The Spitzer Infrared Nearby Galaxies Survey, 2007, Fitfth Enhanced Data Release, see Kennicutt et al. 2003 for a complete description; SDSS-DR7: Sloan Digital Sky Survey Data Release 7, see Abazajian et al. 2009; D09: Dale et al. 2009; S10: Sheth et al. 2010; J04: James et al. 2004; L07: Lira et al. 2007; T05: Taylor et al. 2005; SEIP: The Spitzer Enhancing Imaging Products Database [http://irsa.ipac.caltech.edu/data/SPITZER/Enhanced/SEIP/]).

(Makarov et al. 2014). Although some of these galaxies were classified as barred (SBc) galaxies in some catalogs, there is no strong evidence for bars except in NGC 6503, which contains a faint end-on bar (Kuzio de Naray et al. 2012). NGC 3621 is representative of a pure-disc galaxy, with multiple spiral arms. It is clear from the 3.6μm image that NGC 4605 is not axisymmetrical. The deprojected Hα image of NGC 4605 shows a bisymmetric morphology and perhaps a central elongated structure. However, due to the relatively high inclination of NGC 4605, the resultant bar-like morphology in the deprojected Hα image could be somewhat spurious. Indeed, Simon et al. (2005, hereafter S05) did not find any strong evidence for a bar in NGC 4605. The 3.6μm and Hα images show multiple spiral arms in NGC 5963. This galaxy also shows an elongated structure about 0.25 kpc across. However, it is probably a pseudobulge, not a bar (S05). NGC 5949 has a more flocculent morphology, with less delineated spiral arms. The high inclination of NGC 6689 precludes determining details of its structure, though a deprojection shows signs of spiral-like structure both in the 3.6μm and Hα images. There is no kinematic evidence for a bar (see below).

To carry out the mass models, the photometric and kinematical data were taken from de Blok et al. (2008, hereafter dB08) for NGC 3621, from SO5 for NGC 4605, 5949, 5963 and 6689 and, from Kuzio de Naray et al. (2012)) for NGC 6503. S05 applied multicolour imaging to measure the isophotal parameters of the galaxies. dB08 used the observed 3.6μm surface brightness profile and Kuzio de Naray et al. (2012) used the K_s-band. These bands are considered good tracers of stellar mass.

NGC 3621 is a galaxy included in the H I Nearby Galaxy Survey (THINGS) described in Walter et al. (2008), which consists of high-resolution H I observations of a sample of 34 nearby galaxies. For NGC 5949 and NGC 6689, S05 used Hα two-dimensional velocity fields to derive the rotation curves. For NGC 4605, 5963 and 6503, Hα and CO observations were combined (S05; Kuzio de Naray et al. 2012). The kinematic and photometric values of the PA, centre and inclination angle agree within the uncertainties. Interestingly, S05 used a technique to incorporate the uncertainties of the PA, inclination and centre position, obtaining more realistic rotation curve error bars than just propagating only the uncertainties in the measure of the velocities from each spectrum. Spano et al. (2008) also measured the Hα rotation curve of NGC 5949 and obtained an almost identical rotation curve as S05.

The tilted-ring models allowed to extract the rotational, radial and systemic velocities as a function of radius from the velocity fields. This is done by decomposing the velocity field in Fourier components along the azimuthal angle θ. In a purely axisymmetric galaxy, only the components $\cos\theta$ (rotation) and $\sin\theta$ (radial velocity) are nonzero. The higher order terms (e.g. $\cos 2\theta$, $\sin 2\theta$ and so on), if present, are consequence of non-axisymmetric perturbations in the velocity field, such a bars or spiral arms. For the S05 galaxies, S05 found that the amplitude of the higher order components is not large enough to affect the derived rotation curve. Moreover, this also suggests that bars, if present, are too weak to significantly disturb the kinematics of the gas.

For the galaxies studied, the non-circular motions are dominated by the radial component. Still, the radial motions are so small for NGC 3621, 5949, 6503 and 6689 that can be described by rotation only. In the case of NGC 6689, no deviations from circular motions were detected. This implies that if it has a bar, it should be very faint. The radial motions are moderate in NGC 5963. NGC 4605 is the only galaxy in the sample that deviates significantly from axisymmetry (S05). The radial motions were interpreted as the result of the gas being in elliptical orbits due to the influence of a triaxial dark matter halo (S05).

The observed rotation curves for these galaxies are shown in Figure 4. NGC 4605, 5949 and 6689 exhibit gently rising rotation curves. In the interval plotted, the maximum circular velocities lie between 100 km s^{-1} and 140 km s^{-1}. In the case of NGC 4605, Rubin et al. (1980) already measured the Hα rotation velocity. Their observations extend a bit further, finding a rotational velocity of 100 km s^{-1} at 3.3 kpc in radius. For the galaxies NGC 3621, 5963 and 6503, the H I rotation curves extend up to 23 kpc, 10.5 kpc and 12.2 kpc, respectively (Bosma et al. 1988; dB08; Greisen et al. 2009; Kuzio de Naray et al. 2012). These studies show a flat rotation velocity of 150 km s^{-1} in NGC 3621, 130 km s^{-1} in NGC 5963 and 116 km s^{-1} in the case of NGC 6503.

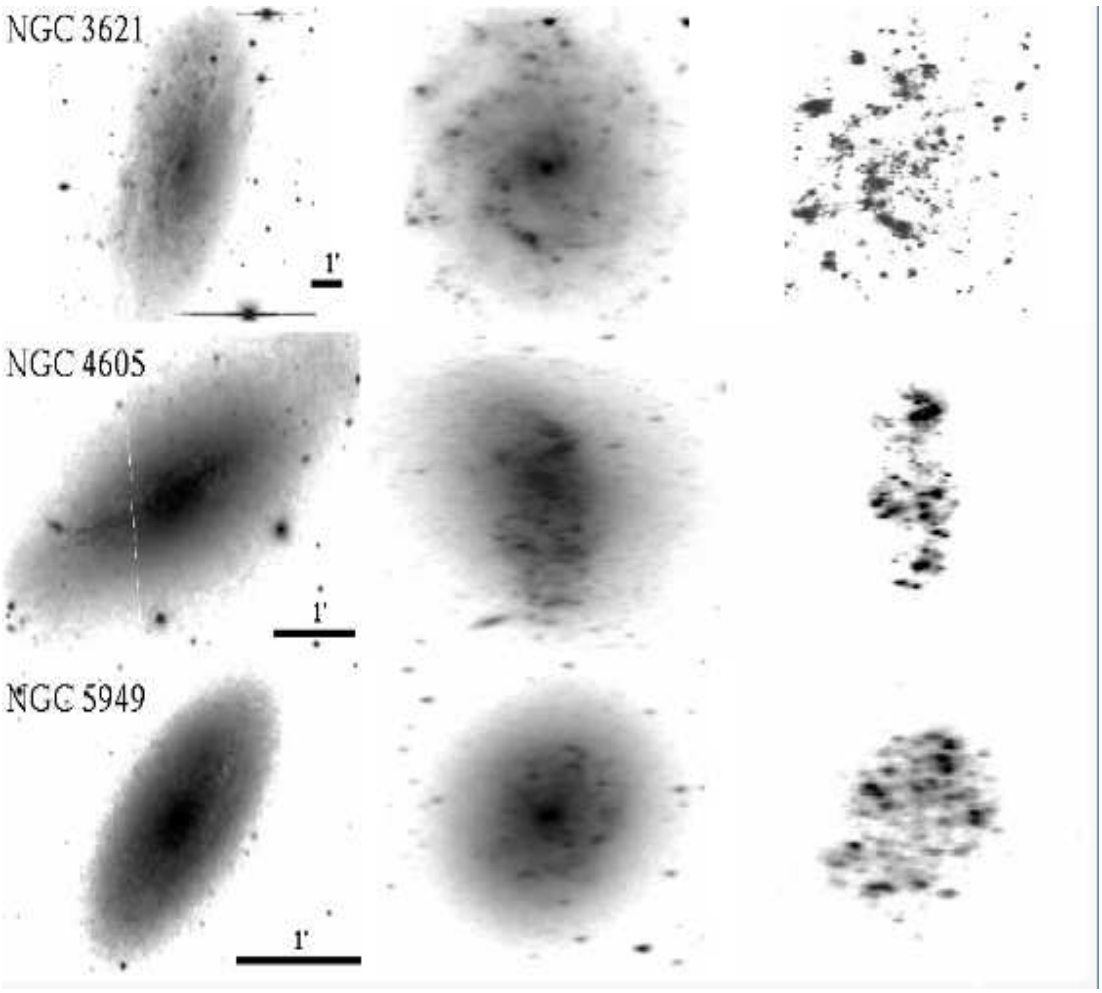

Figure 2. Morphology of NGC 3621, 4605 and 5949 in different bands. Left panels: Three-band (BVR/gri) optical images oriented according to the astronomical convention (North up and East left). Middle panels: Deprojected Spitzer IRAC 3.6μm images. Right panels: Deprojected continuum-subtracted Hα images. All images are displayed in logarithmic gray scale. See Table 1 for the relevant references and databases used.

4 NEWTONIAN ANALYSIS

4.1 Rotation curves and dark matter content

Detailed Newtonian mass models for NGC 3621 can be found in dB08 (see also Randriamampandry & Carignan 2014). Mass models for NGC 4605, 5949, 5963 and 6689 were presented in S05. On the other hand, the galaxy NGC 6503 has been extensively studied in the literature because the observed velocity dispersion profile imposes additional constraints to the surface density of the disc (Bottema 1989; Bottema & Gerritsen 1997; Fuchs 1999; Puglielli et al. 2010). The reader is referred to those papers for the details on the different dark matter mass models. Here we provide the rotation curves in dark matter models because they are useful as the basis of reference in making comparisons.

The light profiles were not decomposed into a disc and a bulge component because all the galaxies are bulgeless except NGC 6503, which contains a small pseudobulge. In this galaxy, the contribution of the pseudobulge to the total galaxy light is only 5 percent (Kuzio de Naray et al. 2012) and its contribution to the circular velocity is appreciable only within a radius of 200 pc. Thus, we can savely neglect the bulge in the mass budget.

Following S05, the surface brightness corrected for inclination in the R-band is used as the reference band for NGC 4605, 5949 and 5963, and the r'-band for NGC 6689. For NGC 3621 and NGC 6503, we will use the 3.6μm and the K_s-band, respectively. The contribution of the baryonic disc to the rotation curve in NGC 4605, 5949, 5963, 6503 and 6689 was computed assuming that the discs are infinitesimally thin and that the stellar mass-to-light ratios, $\Upsilon_\star$, in each band are constant with radius. For NGC 3621, we followed dB08 who took into account radial $\Upsilon_\star$ variations within the stellar disc and assumed a vertical scale height of the stellar disc of one fifth the radial scale length.

In all the galaxies of our sample, the contribution of the gas disc to the rotation curve is small; at those radii under consideration, its effect is similar to a 20% change in $\Upsilon_\star$ (Bolatto et al. 2002; Simon et al. 2003) and, moreover, this decrease could be partly offset by allowing the stellar disc to have a finite thickness (S05). In particular, the contribution of the gas to the rotation curve is $\lesssim 20$ km s^{-1} at the last measured radius (4 kpc) in NGC 5963 (Bosma et al. 1988). Only beyond 10 kpc, the contribution of the gas is non-negligible as compared to the contribution of the stellar disc. Adams et al. (2014) estimated that the contribution of the gas to the NGC 5949 rotation curve is < 20 km s^{-1} if the gas distribution follows the stellar distribution.

Figure 4 shows the fits to the rotation curves, assuming that the dark matter haloes follow a pseudo-isothermal sphere, whose

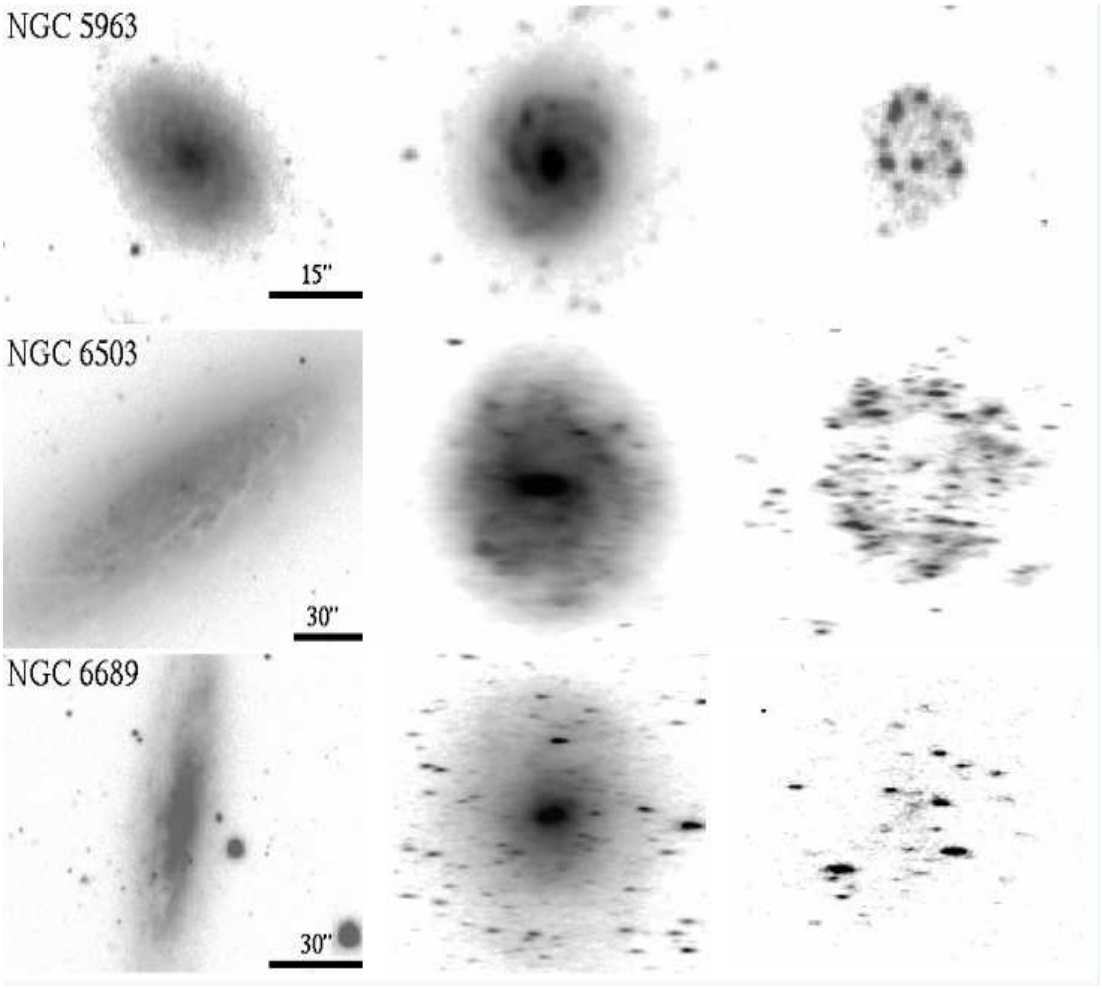

Figure 3. Same as Figure 2 but for NGC 5963, 6503 and 6689. See Table 1 for the relevant references and databases used.

profile is

$$\rho_{\rm ISO}(r) = \frac{\rho_0}{1+(r/R_c)^2}, \qquad (10)$$

where ρ_0 is the central density of the halo and R_c the core radius. Although cosmological simulations predict NFW profiles, it is likely that fluctuations in the gravitational potential caused by bursts of star formation in low-mass galaxies are able to transform initial NFW profiles into cored profiles (e.g., Pontzen & Governato 2014). For NGC 3621, 4605, 5949, 5963 and 6689, we adopt the values of $\Upsilon_\star$ derived by dB08 and S05 using the colour-$\Upsilon_\star$ relations as predicted in population synthesis models and denoted by $\Upsilon_\star^{\rm syn}$ (see Table 2). For NGC 6503, we choose $\Upsilon_{\star,Ks} = 0.24$, for reasons that will become clear later in §5.1. Hence the fits have two free parameters (ρ_0 and R_c). The best-fitting parameters were reported in dB08 and S05. Although the fits are satisfactory in general, a more cuspy profile than the pseudoisothermal distribution leads to better fits in NGC 5963 and NGC 6503. According to Figure 4, NGC 4605, 5963 and 6689 are dark matter dominated galaxies. In NGC 3621, 5949 and 6503, the contribution of the dark matter halo to the rotation curve is comparable to the contribution of the baryonic disc, at least at the galactocentric distances under consideration. In these mass models, NGC 3621 and NGC 4605 have maximum disc mass-to-light ratios. We need to see if the adopted $\Upsilon_\star$-values are consistent with bar-stability constraints. This will be done in the next Section.

Table 2. Summary of stability parameters using a pseudo-isothermal dark matter halo. The suggested range for $\Upsilon_\star$ in column 2 comes from dB08 and S05. In the case of NGC 3621, the two extreme values in the range corresponds to Kroupa and diet-Salpeter initial mass functions. The asterisk indicates that the value used was not derived from the colour-$\Upsilon_\star$ relation.

Name NGC	Suggested $\Upsilon_\star^{\rm syn}$ range	Adopted $\Upsilon_\star^{\rm syn}$	$\langle X_2 \rangle$ using $\Upsilon_\star^{\rm syn}$	$\Upsilon_\star^{\rm (ENL)}$	$\Upsilon_\star^{\rm (PWC)}$
3621	$0.42-0.59$	0.59	1.2	0.27	0.25
4605	$0.94-1.09$	1.01	2.9	1.14	1.06
5949	$1.48-1.80$	1.64	2.0	0.96	1.24
5963	$1.09-1.38$	1.24	2.3	1.00	1.00
6503	–	0.24*	1.9	0.13	0.16
6689	1.96	1.96	3.3	2.92	2.50

4.2 Bar-stability constraints on $\Upsilon_\star$

We computed $\Upsilon_\star^{\rm (ENL)}$ by fitting the rotation curve of each galaxy with progressively lower values of $\Upsilon_\star$ until the condition $\mathcal{R} = 1.1$ was met. The value of $\Upsilon_\star^{\rm (ENL)}$ for the galaxies in question are listed

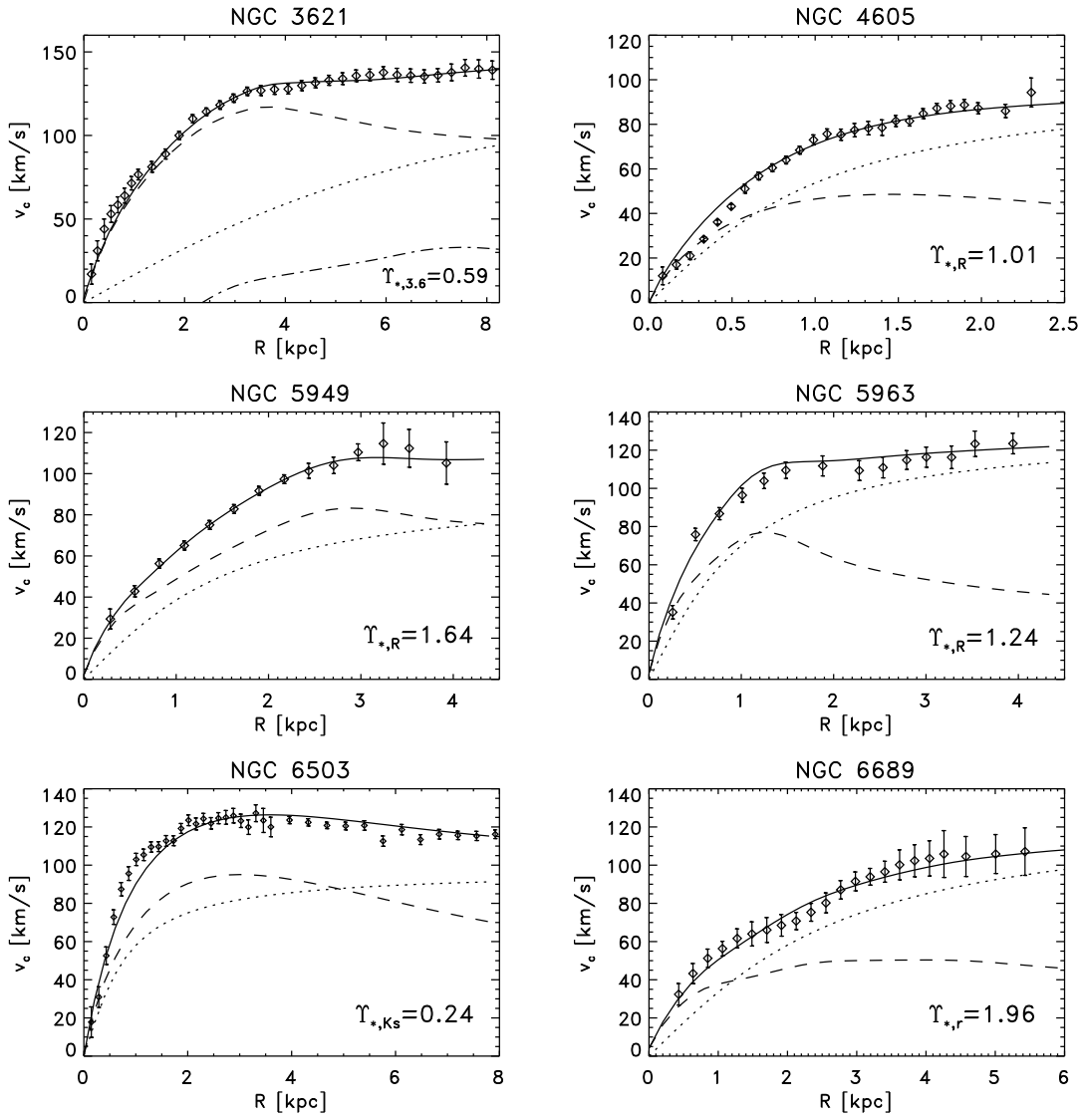

Figure 4. Fits to the observed rotation curves using a pseudo-isothermal profile for the dark matter halo. The dashed line represents the contribution to the rotation curve of the stellar disc using $\Upsilon_\star^{\rm syn}$ given in Table 2. The dotted line shows the contribution of the dark halo and the dot-dashed line indicates the gas contribution.

in Table 2. We see that $\Upsilon_\star^{\rm syn} > \Upsilon_\star^{\rm (ENL)}$ in four galaxies and, according to the ENL criterion, they would be bar unstable when assuming $\Upsilon_\star^{\rm syn}$, which is the mean value derived from population synthesis models. However, only for two galaxies (NGC 3621 and NGC 5949), $\Upsilon_\star^{\rm (ENL)}$ is well below the range suggested by population synthesis models.

In order to compute $\Upsilon_\star^{\rm (PWC)}$, we have derived X_2 versus R for our six galaxies under consideration, and for the mass models presented in Section 4.1 (having $\Upsilon_\star$-values as indicated by galaxy colours). The radial profile of X_2 is shown in Figure 5, where the radius is normalized in terms of the scale length of the disc h_R. Since the radial brightness profile of the disc in some galaxies is not perfectly exponential, we have defined $2h_R$ as the galactocentric distance where the mass surface density drops a factor of $\exp(2)$ from its central value. We see that NGC 3621 exhibits the lower values of X_2.

Since the four S05 galaxies and NGC 3621 exhibit no indication of a strong bar, we may conservatively assume that for these five galaxies it holds that $\langle X_2 \rangle > 2.7$. The resultant $\Upsilon_\star^{\rm (PWC)}$ values in our galaxies are given in Table 2.

We see that $\Upsilon_\star^{\rm (ENL)}$ and $\Upsilon_\star^{\rm (PWC)}$ are not dissimilar; it holds that

$$0.85 \leq \frac{\Upsilon_\star^{\rm (PWC)}}{\Upsilon_\star^{\rm (ENL)}} \leq 1.3. \qquad (11)$$

For the five galaxies with empirical determinations of $\Upsilon_\star^{\rm syn}$ from galaxy colours, $\Upsilon_\star^{\rm (ENL)}$ and $\Upsilon_\star^{\rm (PWC)}$ are significanly smaller than those values predicted from population synthesis models in two galaxies: NGC 3621 and NGC 5949. The $\Upsilon_\star^{\rm syn}$-value in NGC 3621 is a factor of 1.5-2 larger than the upper value inferred to have bar stability. However, several assumptions have to be made to compute $\Upsilon_{\rm syn}$, such as the choice of the initial stellar mass function or the star formation history, which may account for this discrepancy (see Conroy 2013, for a review). For NGC 5949, values of $\Upsilon_{\star,R}$ larger

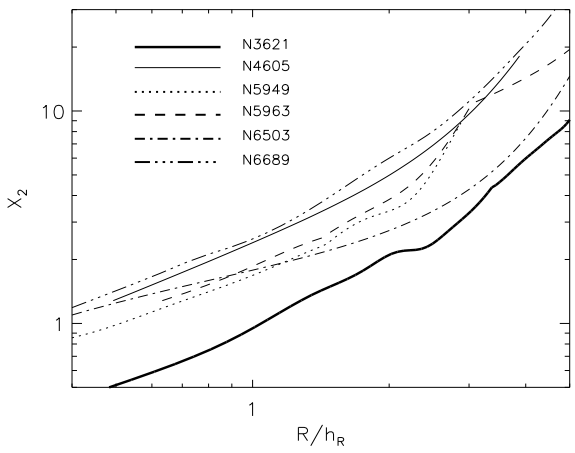

Figure 5. Radial profile of X_2 for those Newtonian mass models (stellar disc plus pseudo-isothermal dark halo) shown in Figure 4.

than ~ 1.3 are not permitted from the stability analysis. Interestingly, Adams et al. (2014) derived the best-fitting value of $\Upsilon_{\star,r}$ in NGC 5949 from kinematic models and found that it is 1.16 ± 0.34 when gas-based models are used, and 1.20 ± 0.28 when the stellar kinematics is used instead.

The stability of one galaxy of our sample, NGC 6503, has been examined in great detail in the literature. Bottema & Gerritsen (1997) concluded that the peak of the contribution of the disc to the rotation curve cannot contribute more than 90 km s^{-1} in NGC 6503 because the disc would develop a prominent (unobserved) bar. This condition implies that $\Upsilon_{\star,Ks} \leq 0.21$. The knowledge of the line-of-sight velocity dispersion profile allows a more sophisticated analysis. Bottema & Gerritsen (1997) found that the relatively low values of the observed velocity dispersion are reproduced in the simulated galaxy when the disc contributes $\sim$ 70 km s^{-1} at its peak (or, equivalently, $\Upsilon_{\star,Ks} \leq 0.13$). Therefore, the values of $\Upsilon_\star^{(\mathrm{ENL})}$ and $\Upsilon_\star^{(\mathrm{PWC})}$ obtained for NGC 6503 are consistent with these previous estimates.

In summary, we find that (1) $\Upsilon_\star^{(\mathrm{ENL})}$ and $\Upsilon_\star^{(\mathrm{PWC})}$ are not dissimilar and (2) in two of the galaxies the values for $\Upsilon_\star$ suggested by population-synthesis models are a factor of $1.5 - 2$ larger than those values allowed by bar-stability arguments.

4.3 A note on the spiral arm multiplicity

The number of spiral arms may also set constraints on $\Upsilon_\star$. This kind of analysis is adequate for galaxies having low inclinations in order to trace out correctly the spiral arms (e.g., D'Onghia 2015). As discussed in §3, some of the galaxies in our sample exhibit a multi-armed shape (NGC 3621 and NGC 5963). In particular, NGC 5963, the galaxy with the less inclination in our sample, shows the presence of four tightly wound spiral arms. Thus, the surface density in this galaxy should be small enough for the the amplification of bisymmetric ($m = 2$) modes to be highly suppressed. Assuming $\alpha = 1.5$ (see §2.1.1) and a stellar disc with $\Upsilon_\star = 1.0$ (see previous Section), the $m = 4$ mode is efficiently swing amplified from $0.8h_R$ (or ~ 0.55 kpc) to $1.5h_R$ (or 1.0 kpc). This dominance of the $m = 4$ mode may be consistent with the spiral morphology seen in the optical images (see Figure 3 in the present paper and Figure 1c in S05), although the 3.6μm image shows that two arms are more prominent than the other two.

Table 3. Summary of stability parameters using MOND. The quoted intervals in $\Upsilon_\star^{\mathrm{fit}}$ and $\langle X_2 \rangle$ correspond to the 95% posterior credible bands. The range for $\Upsilon_\star^{\mathrm{syn}}$ in column 2 comes from dB08 and S05. In the case of NGC 3621, the two extreme values in the range corresponds to Kroupa and diet-Salpeter initial mass functions.

Name	$\Upsilon_\star^{\mathrm{syn}}$ range	$\Upsilon_\star^{\mathrm{fit}}$	$\mathcal{R}$	$\langle X_2 \rangle$ using $\Upsilon_\star^{\mathrm{fit}}$
NGC 3621	$0.42 - 0.59$	0.401 ± 0.014	0.92	1.39 ± 0.04
NGC 4605	$0.94 - 1.09$	$1.010^{+0.066}_{-0.056}$	0.96	$1.57^{+0.08}_{-0.09}$
NGC 5949	$1.48 - 1.80$	$1.444^{+0.146}_{-0.143}$	0.87	$1.70^{+0.17}_{-0.14}$
NGC 5963	$1.09 - 1.38$	$1.910^{+0.241}_{-0.255}$	0.73	$1.32^{+0.19}_{-0.14}$
NGC 6503	–	0.24 ± 0.012	0.82	$1.47^{+0.07}_{-0.06}$
NGC 6689	1.96	$2.366^{+0.455}_{-0.424}$	1.10	$1.84^{+0.36}_{-0.27}$

5 ANALYSIS IN MOND

5.1 MOND fits to the rotation curves

Fits to the rotation curves of NGC 3621 using MOND can be found in Gentile et al. (2011), Angus et al. (2012) and Randriamampandry & Carignan (2014). These authors used the same THINGS data as we adopt here. The rotation curve of NGC 6503 was studied in the MOND context by Bottema & Pestaña (2015).

In both formalisms described in Section 2.2 (the non-linear Poisson equation and QUMOND), the following algebraic relation between the 'true' acceleration g_M and the Newtonian acceleration g_N (created by the visible components) is a good approximation in the midplane of smooth axisymmetric disc systems

$$\mu\left(\frac{|\boldsymbol{g}_M|}{a_0}\right)\boldsymbol{g}_M = \boldsymbol{g}_N \tag{12}$$

(Milgrom 1986; Angus et al. 2012). Equation (12) relates the MOND circular velocity $v_{c,M} = (g_M R)^{1/2}$ to the Newtonian circular velocity $v_{c,N} \equiv (g_N R)^{1/2}$ as

$$\mu(x) v_{c,M}^2 = v_{c,N}^2, \tag{13}$$

with

$$x = \frac{v_{c,M}^2}{R a_0}. \tag{14}$$

Famaey & Binney (2005) found that the "simple" μ-function, $\mu = x/(1+x)$, fits the data of NGC 3198 and the terminal-velocity curve of the Milky Way much more satisfactorily than the standard interpolating function. Famaey et al. (2007) and Sanders & Noordermeer (2007) also found that the simple μ-function provides more plausible values of the relative stellar mass-to-light ratios for bulge and disc, as well as the generally smaller global mass-to-light ratio, for a sample of galaxies having a gradual transition from the Newtonian limit in the inner regions to the MOND limit in the outer parts. For the galaxies in the sample of Gentile et al. (2011), the simple interpolating function also yields better fits to the rotation curves than the standard interpolating function (see also Weijmans et al. 2008).

Figure 6 shows the fits to the rotation curves using the MOND framework with the simple interpolating μ-function. The Newtonian circular velocities $v_{c,N}$ (without dark matter) were determined

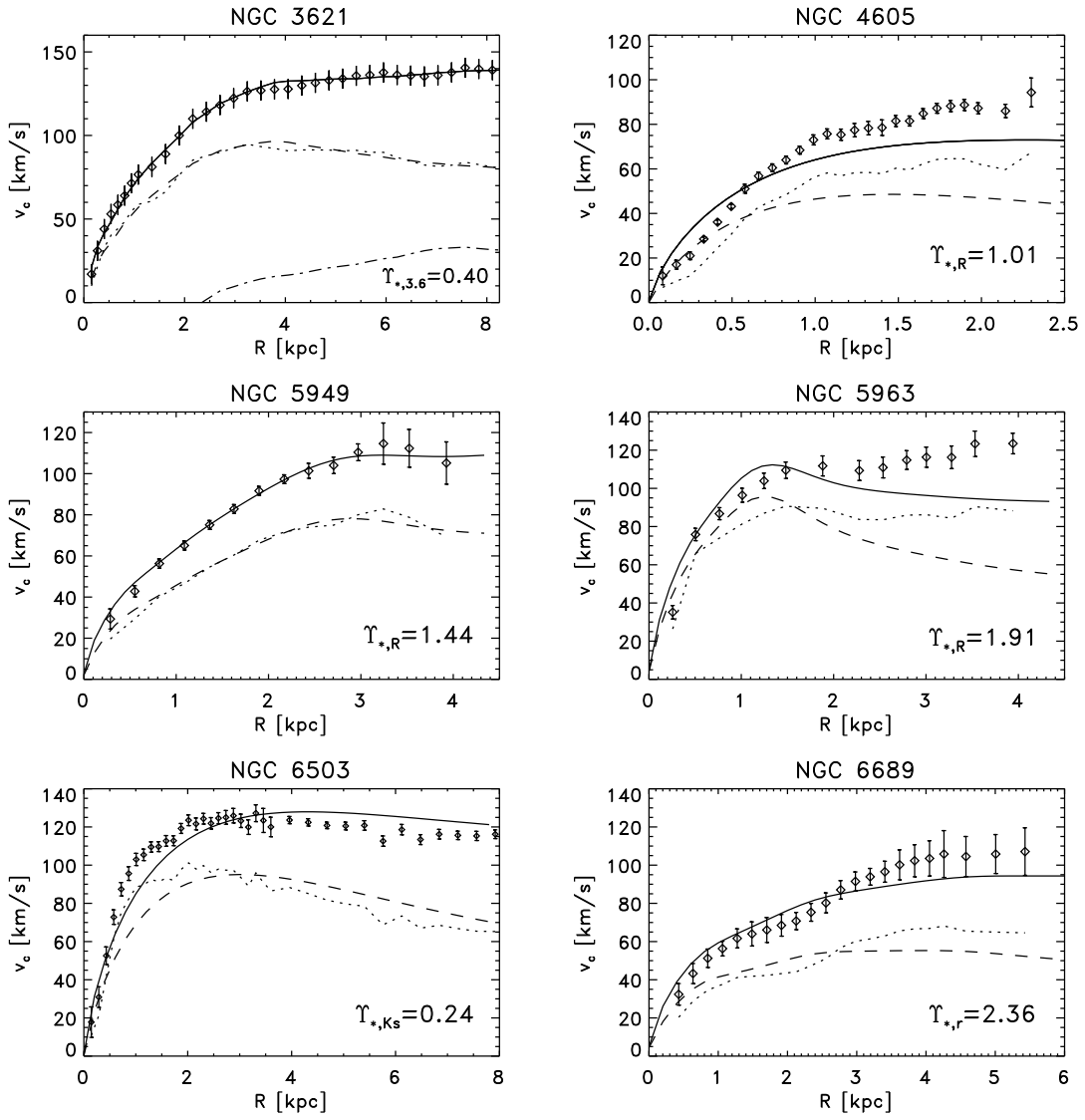

Figure 6. MOND fits to the observed rotation curves using the simple μ-function with $a_0 = 1.2 \times 10^{-8}$ cm s^{-2} and treating $\Upsilon_\star$ as free parameter, which is quoted at the right corner at each panel. The dashed curves represent the Newtonian contribution of the stellar disc. The dotted lines indicate the contribution of the stellar disc required by MOND in order to have a perfect fit to the observed rotation curve.

as described in §4.1. We made fits with $a_0 = 1.2 \times 10^{-8}$ cm s^{-2} and only $\Upsilon_\star$ as a free parameter. The required stellar mass-to-light ratios in the four S05 galaxies obtained in the fit to the rotation curves ($\Upsilon_\star^{\rm fit}$) are given in Table 3. The intervals shown in this Table correspond to 95% posterior credibility intervals obtained using the Bayesian inference method presented in Appendix C. The $\Upsilon_\star^{\rm fit}$ values are consistent with those derived using the colour-$\Upsilon_\star$ relations predicted in population synthesis models except for NGC 5963 (see Table 3). The relatively large values of g_M/a_0 in NGC 5963 yield a $\Upsilon_\star^{\rm fit}$-value close to the maximum disc mass-to-light ratio.

We see that the fit is good for NGC 3621 and NGC 5949, acceptable for NGC 6689, but poor for NGC 4605, 5963 and 6503. In order to highlight the significance of the MOND fits, the dotted lines in Figure 6 show the radial profiles of the Newtonian circular velocity required to match the observed rotation curve with MOND. It is a complementary way to quantify what MOND requires to provide a successful fit. We see that for NGC 4605 and NGC 5963, the discrepancy between the required and the observed Newtonian circular velocities is significant.

Although a_0 and the interpolating function should be universal, they must be determined empirically. Interestingly, in galaxies having $x \gtrsim 1$ at every observed radius, or galaxies with x constant along R, the shape of the rotation curve predicted by MOND is barely sensitive to the particular choice of the interpolating function or on the adopted value of a_0. According to Equation (13), for those galaxies, MOND predicts that the rotation curve should be a scaled version of the Newtonian rotation curve. Figure 7 shows $x = v_c^2/(Ra_0)$, with v_c the observed rotation curve. We see that for NGC 5949 and NGC 6689, x is approximately constant with radius. For NGC 5963, $x \gtrsim 1$ at all the observed galactocentric distances. Thus, for these three galaxies, the fit to the rotation curves are expected to be insensitive to small changes to the adopted value of a_0 or the exact form of the interpolating function. In fact, we recalculated the fits for $a_0 = 0.9 \times 10^{-8}$ cm s^{-2} and for 1.2×10^{-8} cm s^{-2}, leaving $\Upsilon_\star$ as the free parameter. Using these values for

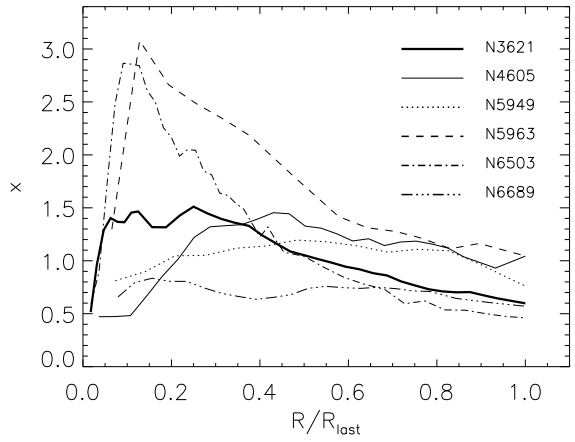

Figure 7. Observed radial acceleration divided by a_0 (see Equation 14) versus R for each galaxy. $R_{\rm 1last}$ is the radius of the last radial point in Figure 6.

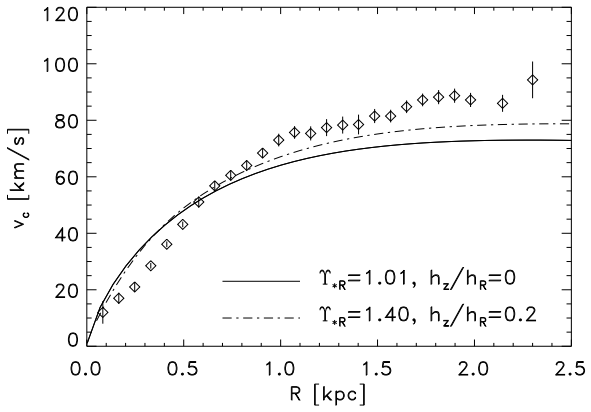

Figure 8. The difference in the MOND rotation curves for NGC 4605 in the case of null thickness (solid line) and a finite thickness (dot-dashed line) of the stellar disc.

a_0, the differences in the circular velocity are less than 3%, making them barely distinguishable.

We have explored other values of the index n in the interpolating function (see Eq. 6), and found that $\Upsilon_\star$ does depend on the value of n, but the quality of the fits to the rotation curves are rather insensitive. None n-value provides satisfactory fits to the rotation curves of all the galaxies in our sample. Since $n = 1$ provides $\Upsilon_\star$-values very close to what the colour-$\Upsilon_\star$ relation predicts (see also Famaey et al. 2007), we restrict our analysis to the simple μ-function in the remainder of the paper.

Distances to the galaxies are another source of uncertainty (see Table 1 for the estimated uncertainties in the distances). It is easy to show that it is equivalent to vary D by a factor of α (with a_0 fixed) than changing a_0 by the same factor α (with D fixed). We find that the goodness of the fits to the rotation curves is almost unaltered if the distance to these galaxies is allowed to vary by 15 percent.

The uncertainty in the distance of NGC 5949 could be significantly larger than 15%. For this galaxy, S05 derived a distance of 14.0 ± 2.4 Mpc from the Tully-Fisher relation. Adams et al. (2014) reported a distance of 14.3 Mpc implied by the Hubble flow, whereas Spano et al. (2008) assumed a distance of 7.4 Mpc. Fortunately, for this galaxy, x is approximately constant with galactocentric radius and hence the goodness of the fit to the rotation curves is not very sensitive to the adopted distance.

Figures 6 indicates that in the central regions of NGC 4605, 5963 and 6689, MOND predicts higher rotation speeds than observed. A slightly better fit to the rotation curves of these galaxies can be achieved by including the finite thickness of stellar discs. Figure 8 shows the MOND rotation curve for NGC 4605 with $\Upsilon_{\star,R} = 1.4$, when the Newtonian acceleration at the midplane was calculated assuming that the stellar scale height is one fifth the stellar scale length. The fit is still not fully satisfactory; the MOND fit within $R = 2.4$ kpc predicts an asymptotic value of 80 km s^{-1}, which is significantly below the circular velocity of 100 km s^{-1} measured by Rubin et al. (1980) at 3.3 kpc. However, uncertainties in the ellipticity caused by the non-axisymmetric structures seen in both photometric and kinematic maps (see Figure 2 and S05) might be the reason why MOND does not correctly predict the rotation curve of NGC 4605.

MOND is also unable to reproduce the shape of the rotation curve of NGC 5963; the observed rotation curve at the peak of the disc is still rising, but MOND predicts that it should slowly drop in a similar fashion as the Newtonian circular velocity does, because $x > 1$. This feature is also present in other galaxies. For instance, the compact galaxies UGC 5721, 7399, 8190 and 9179 also exhibit a rising of the rotation curve beyond the turnover of the Newtonian rotation curve (Spano et al. 2008; Swaters et al. 2010), which MOND cannot reproduce (e.g., Swaters et al. 2010). Although the rotation curves of UGC 5721, 7399 and 8490 were classified as high quality, based on asymmetry, bar, and so on, Swaters et al (2010) identified twisting isophotes in the central regions of UGC 5721 (suggesting the presence of non-circular motions), the bar in UGC 7399, and the large warp in UGC 8490 as possible agents which may affect the derived rotation curve. The galaxy NGC 5963 also contains non-circular motions of the order of ~ 15 km s^{-1} (S05), which may affect the observed rotation curve at $R > 3$ kpc.

Moreover, the peculiar surface brightness map of NGC 5963, showing a steep decline beyond ~ 1 kpc, may indicate that the assumption of a constant $\Upsilon_\star$ across this galaxy is not a good approximation. The surface brightness profile may be modelled by the sum of two exponential components, each of them having different $\Upsilon_\star$. Using a double exponential profile, the MOND fit to the rotation curve is slightly improved.

In NGC 5963, the asymptotic velocity predicted using our MOND fit to the rotation curve is 98 km s^{-1}, small as compared to the asymptotic velocity measured by Bosma et al. (1988). However, we have neglected the gas mass, which is significant at larger radii. By including the gas mass, the asymptotic circular velocity expected under MOND, $(GMa_0)^{1/4}$, is larger.

In NGC 6503, MOND underpredicts the circular speed at the radial interval 0.8 kpc $< R < 2.5$ kpc. If the dust obscures part of the light, this discrepancy may be expected because of our poor correction for dust extinction. Bottema (1989) suggested that dust extinction could be responsible for the plateau observed between $R = 0.1$ kpc and $R = 1$ kpc in B- and R-band surface brightness profiles. For NGC 6503, we have made a fit with both $\Upsilon_{\star,Ks}$ and the scale length of the exponential stellar disc h_R, as free parameters. The best fitting parameters were found to be $\Upsilon_{\star,Ks} = 0.35 \pm 0.017$ and $h_R = 1.06 \pm 0.03$ kpc. Nevertheless, this hypothesis that the light distribution does not trace the underlying mass distribution due to the presence of dust, has been ruled out by Kuzio de Naray et al. (2012) on the basis that the plateau is

also present in the K_s-band photometry and on the agreement between Hα and CO rotation curves, which suggests that extinction is minimal.

5.2 The X_m-parameter in the MOND framework

Figure 9 shows the MOND X_2 parameter as a function of R for the galaxies in our sample, when the simple μ-function is used: $\mu(x) = x/(1+x)$ and $L(x) = 1/(1+x)$. We see that the values of X_2 at a given R/h_R vary little from galaxy to galaxy.

In Section 5.1, we found that the MOND fits to the rotation curves for NGC 4605 and NGC 5963 are clearly unsatisfactory and thus any further analysis will be relevant once we can identify the cause of this discrepancy. If the explanation for the poor fit to the rotation curve is only that the measured rotation curves for these galaxies are affected by the presence of non-circular motions in the gas, we may put aside the rotation curves from the analysis, and recalculate X_2 for reasonable values of $\Upsilon_\star$. Doing so, we find that the radial profile of X_2 is rather insensitive to the adopted value of $\Upsilon_\star$ (see also Section 5.4). For instance, even if we adopt a value twice lower than $\Upsilon_\star^{\rm syn}$, the X_2 parameter increases by less than 15%; the effect is not significant. The reason is that adopting a smaller $\Upsilon_\star$ leads to a smaller surface density but also to a slower rotation and thereby a lower κ, which all together results in a similar X_2.

As a second possibility, we may assume that the measured rotation curves and the quoted error bars are reliable but the mass in the disc of NGC 4605 and NGC 5963 does not follow light (or the photometry analysis is not precise enough to derive the distribution of stellar mass). If MOND is correct, we can derive both the disc surface density and $X_2(R)$ from the observed rotation curve alone. Doing this exercise for NGC 4605, we found that X_2 increases by 11% at a galactocentric distance of $2h_R$ (or 1.36 kpc), and by 30% at $3h_R$ (i.e. 2 kpc). Since the PWC criterion for bar stability depends on the value of X_2 within $2h_R$, the 11% enhancement in X_2 is again not significant as far as bar-stability analysis concerns.

As a summary of this Section, we conclude that for the galaxies in our sample, the profiles of X_2 vs R/h_R are rather similar from galaxy to galaxy. The low values of X_2 in MOND are intrinsic to the basic tenets of MOND. For the galaxies with poor MOND fits to the rotation curves, we have explored other scenarios but find that the MOND values of X_2 are rather robust to observational uncertainties. The analysis for NGC 5963 should be taken with caution because this galaxy has an unusual surface brightness, which may indicate that a constant $\Upsilon_\star$ may not be a good approximation.

5.3 A short comment on arm multiplicity in MOND

In Figure 9, we have also marked the predicted extension of the spiral arms with multiplicity $m = 2$ and $m = 4$ by using that $m = 2\alpha^{-1}X_2$ and $\alpha \simeq 1.25$ for all the galaxies except for NGC 5949, because it has an almost linear rotation curve (see §2.1.1). In the case of NGC 5963, the galaxy discussed in §4.3 because its low inclination allows us to trace out their spiral arms, the swing amplification theory predicts that, under MOND, it should show two spiral arms within $1.3h_R \simeq 0.9$ kpc. From the present analysis, it is not easy to decide if the observed spiral arm multiplicity is consistent with this prediction or not; S05 argued that this galaxy contains four spiral arms in detailed optical images (see figure 1c in S05), which is inconsistent with the MOND prediction that it should exhibit only two arms. On the other hand, the 3.6μm image in Figure 3 shows two prominent spiral arms but also two fainter spiral arms. We remind that the spiral wave theory is implicitely assuming that discs are relatively cold (see §2.1.1). In hot discs, the self-gravity of the disc is weaker and the amplification factor of spiral waves becomes lower. This possibility will be discussed in §5.5.

5.4 Bar instability in MOND

We first consider the ENL stability criterion. The values of $\mathcal{R}$ for the six galaxies in MOND are listed in Table 3. For all galaxies except NGC 6689, $\mathcal{R}$ is less than the critical value 1.1. This implies that these five galaxies are bar unstable not only in the MOND context, but also in the equivalent Newtonian systems. In other words, the values of $\Upsilon_\star$ required to account for the rotation curves in MOND are so large and the discs so massive that these galaxies would be unstable against bar modes even under Newtonian dynamics.

We have computed $\langle X_2\rangle$ in MOND. In Table 3, we provide the values of $\langle X_2\rangle$ and also the 95% posterior credibility interval obtained using the Bayesian approach. The value of $\langle X_2\rangle$ is very insensitive to changes in the adopted inclination angle of the galaxy, distance or observational uncertainties in the rotational velocity. For the galaxies in our sample, $\langle X_2\rangle$ lies between 1.4 and 1.9 (see Table 3). Accordingly, the PWC criterion predicts that all the galaxies should have strong bars, unless the stellar discs are dynamically hot.

Due to the relatively high inclination of NGC 4605, we cannot rule out the existence of bars in this galaxy. One could argue that the noncircular motions detected in NGC 4605 are due to a hidden bar. If the bar is aligned with the major axis, the rotational velocities using standard tilted-ring models are underestimated (e.g. Randriamampandry et al. 2015) and this could explain why the MOND fit to the rotation curve in NGC 4605 is so poor. A more detailed analysis using different wavelengths, as that done for NGC 2976 in Valenzuela et al. (2014), is required to test if this interpretation is correct.

Since there is no evidence for strong bars in any of the galaxies in our sample (see §3), it is worthwhile to explore a scenario where galaxies are stable due to their stellar random motions. This possibility is not new and has been discussed in Sellwood (2016) in a general context. He found that this scenario is unsatisfactory in the case of late-type spirals with stellar masses between $10^8 M_\odot$ and several $10^9 M_\odot$, because these galaxies do not show evidence of strong dynamical heating as far as they do not possess bulge, they are rather thin and display spiral-arm structure, which indicates that they are not so hot to suppress the growth rates for bar instabilities.

5.5 Supression of bar instabilities: dynamically-hot discs?

In this Section, we discuss the magnitude of the velocity dispersion to provide stability. Athanassoula & Sellwood (1986) found that isolated (two-dimensional) Kuzmin-Toomre discs with $\langle Q\rangle \geq 2.2$ are stable to bar instability. In the dynamical models of NGC 6503, Puglielli et al. (2010) also found that a weak bar is developed in models where the minimum Q-value is $\simeq 2.2$.

For each galaxy, we have computed the radial velocity dispersion as a function of R assuming that the MOND Toomre parameter is constant and equal to 2.2 at any galactocentric distance. We have assumed that the galaxies are purely stellar discs. The radial profiles of σ_R are shown in Figure 10. They should be interpreted as the minimum radial velocity dispersions required to guarantee disc stability under MOND theory.

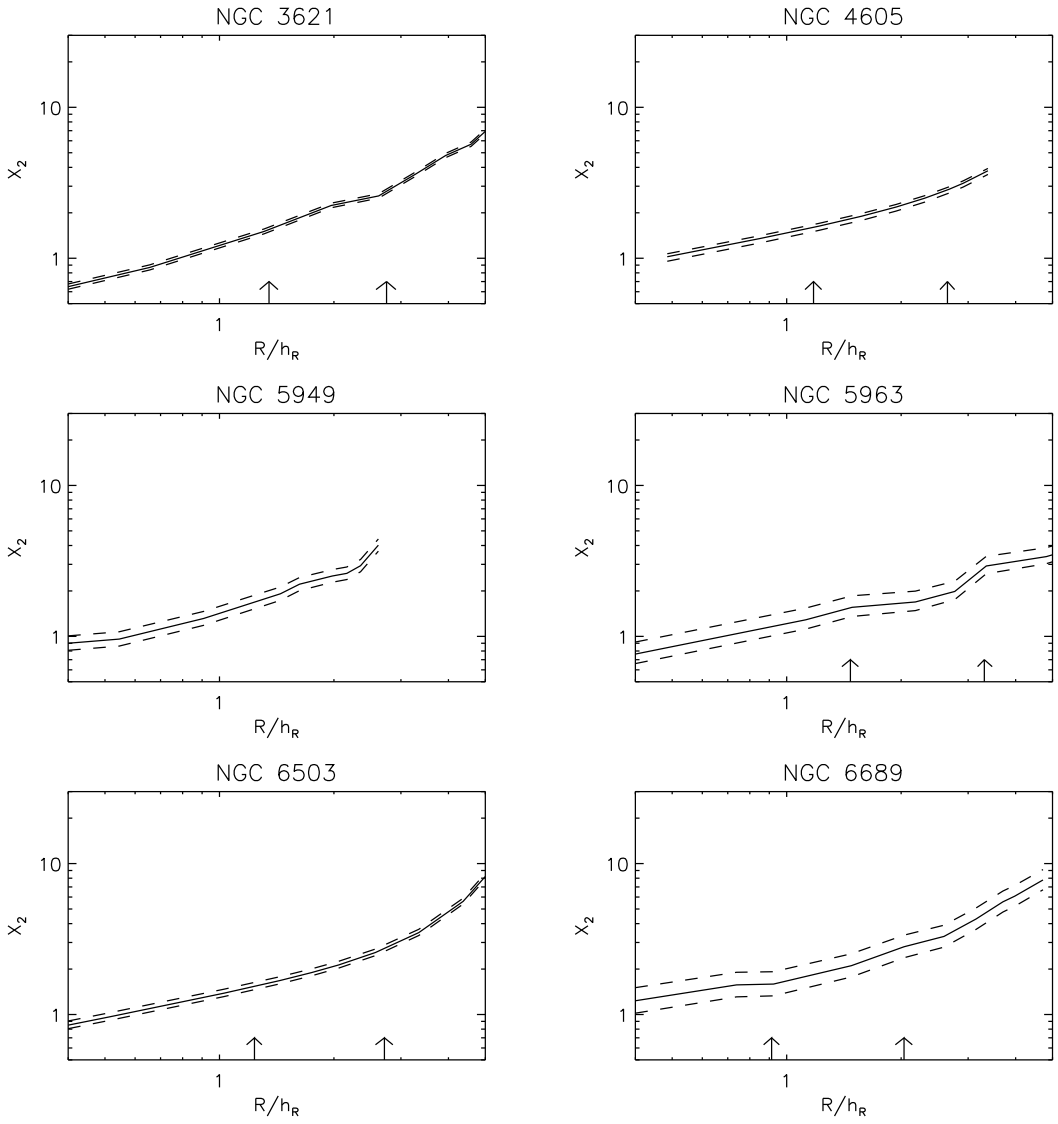

Figure 9. X_2-parameter versus R under MOND (solid line) together with the 95% posterior credible band (dashed lines). We have used the simple μ-function with $a_0 = 1.2 \times 10^{-8}$ cm s^{-2}. The arrows indicate the maximum galactocentric distances where the swing amplification of the modes $m = 2$ (left arrow) and $m = 4$ (right arrow) can occur in each galaxy (except for NGC 5949).

For the galaxies in the present sample, there are measurements of the light-of-sight velocity dispersion only for NGC 6503 (Bottema 1989; Barth et al. 2002; Kormendy et al. 2010). For galaxies with high inclinations as NGC 6503, the line-of-sight velocity dispersion is given by a weighted combination of the radial (σ_R) and tangential (σ_ϕ) components of the velocity dispersion. Using that $\sigma_\phi \simeq 0.7\sigma_R$ from the epicyclic approximation and following Bershady et al. (2010), it is easy to infer that the line-of-sight velocity dispersion, in highly inclined galaxies, is smaller than the radial velocity dispersion by 20% at most (see also Kregel et al. 2005a). Bottema (1989) observed at $5020\mathring{A}$, and the line-of-sight velocity dispersion profile is shown in the corresponding panel in Figure 10. Barth et al. (2002) and Kormendy et al. (2010) observed at $\sim 8500\mathring{A}$ and obtained a larger value of the velocity dispersion in the centre of the galaxy (see Figure 10). The reasons for this discrepancy are still not clear (see Kormendy et al. 2010, for a discussion), but it is likely that they are observing different populations at the centre of the galaxy. Anyway, even adopting the largest values for the line-of-sight velocity dispersions (~ 40 km s^{-1}), NGC 6503 is not dynamically hot enough to assess the level of stability required. Why NGC 6503 does not contain a strong bar has so far defied explanation within MOND.

For the remainder five galaxies, there is no direct measurements of the velocity dispersion, but we may use some correlations derived in other galaxies to evaluate whether the required velocity dispersion to satisfy stability is feasible or not. In fact, observations indicate that those galaxies with higher circular velocity present larger stellar velocity dispersion. For a sample of 11 galaxies, Bottema (1993) found a linear trend between the central value of the vertical velocity dispersion, which we denote by $\sigma_z(0)$ (and it is approximately σ_R at one scalelength) and the galaxy maximum rotation velocity $v_{\rm max}$

$$\sigma_z(0) = \sigma_R(h_R) = (0.29 \pm 0.10) v_{\rm max}. \qquad (15)$$

For a sample of 15 intermediate to late-type edge-on galaxies,

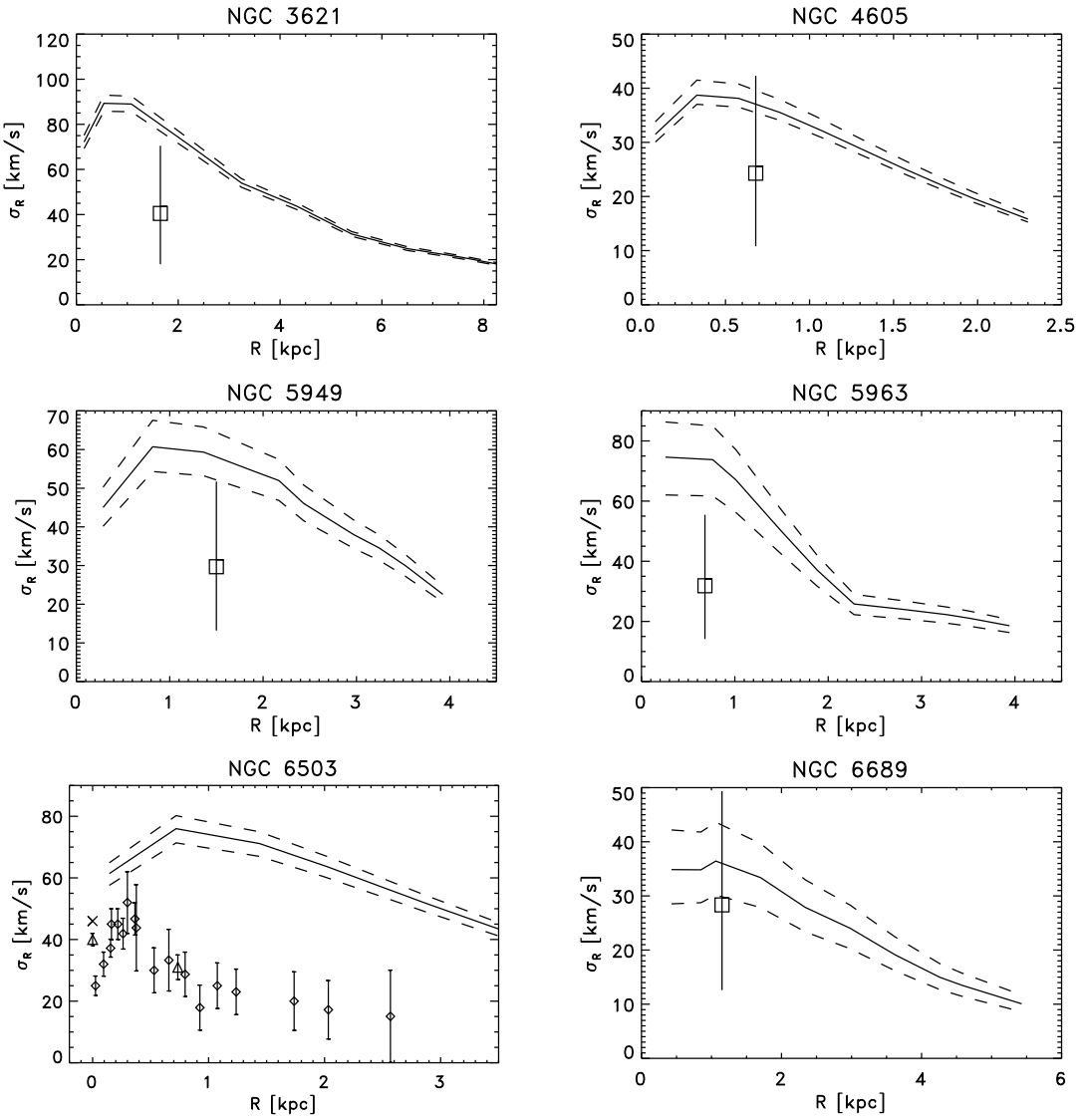

Figure 10. Radial velocity dispersions in order to have a constant Toomre parameter $Q_M = 2.2$ in MOND. The dashed lines show the 95% posterior credible interval. In the case of NGC 6503, the observed line-of-sight velocity dispersion is also shown from Bottema (1989) (diamonds with error bars), Barth et al. (2002) (cross at $R = 0$) and Kormendy et al. (2010) (triangles with error bars). For the remainder four galaxies, we plot the expected σ_R at one scalelength (open square), as derived using a sample of 62 late-type spiral galaxies with published stellar velocity dispersions (see §5.5). The vertical bar indicates the range that contains 95% of the galaxies in these sample of 62 galaxies.

Kregel et al. (2005b) found a similar correlation

$$\sigma_z(0) = \sigma_R(h_R) = (0.22 \pm 0.10) v_{\max} + (10 \pm 17). \quad (16)$$

Moreover, Kregel et al. (2005b) combined all the galaxies with known stellar disc velocity dispersion at that time, gathering a sample of 36 galaxies, which includes from S0-a to Scd galaxies. For that sample of galaxies, they reported that

$$\sigma_z(0) = \sigma_R(h_R) = (0.33 \pm 0.05) v_{\max} + (-2 \pm 10). \quad (17)$$

Finally, for a sample of 30 close to face-on galaxies, Martinsson et al. (2013) found the following relationship

$$\sigma_z(0) = (0.248 \pm 0.038) v_{2.2}, \quad (18)$$

where $v_{2.2}$ is the circular velocity at a radius $2.2 h_R$.

From the above empirical correlations, we infer that galaxies with $v_{\max} = 100$ km s^{-1}, as those galaxies in the present sample, have a mean σ_R at one scalelength of 30 km s^{-1}, with a 1σ scatter of 10 km s^{-1}.

To have a more complete picture of the full sample of galaxies, we have constructed a histogram of the distribution of the parameter $\mathcal{B}$, defined as $\mathcal{B} \equiv \sigma_R(h_R)/v_{\max} \simeq \sigma_z(0)/v_{\max}$, for the total sample of 62 galaxies, consisting of the extended sample of Kregel et al. (2005b) plus the sample in Martinsson et al. (2013), but excluding the four early galaxies of type S0 and Sab (see Figure 11). We find that 95% of the galaxies have $\mathcal{B}$ values in the interval between 0.13 and 0.45. For each galaxy, we have computed this interval for the expected value of σ_R at h_R using the observed value of $v_{\max}$ and they are shown in Figure 10 as an open square and a vertical bar.

In the case of NGC 4605, we already discussed in §5.4 that a more detailed analysis is required to decide if NGC 4605 has a

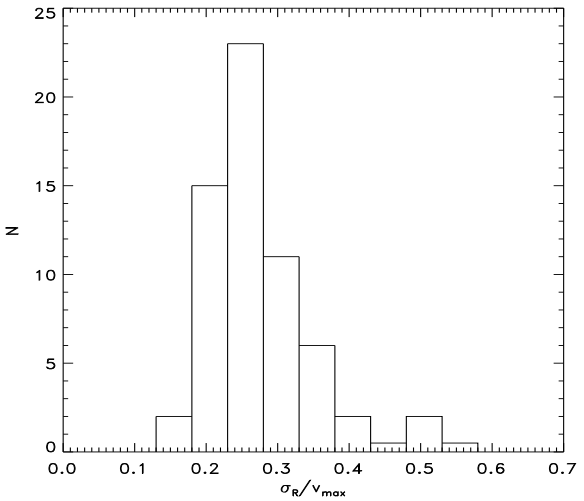

Figure 11. Histogram of $\mathcal{B}$, defined as the ratio between σ_R at h_R and $v_{\rm max}$ (the maximum of the observed rotation curve), for a sample of 62 spiral galaxies.

bar or not. Hence, it remains unclear if this galaxy is stable to bar formation.

From Figure 10, we see that the expected velocity dispersion is fully consistent with the values required to have $Q_M = 2.2$ in NGC 6689. Remind that for this galaxy, there is no any evidence for a bar either photometrically or kinematically. Indeed, S05 did not detect any deviations from circular motions. If the radial velocity dispersion at $1h_R$ is confirmed to be larger than 35 km s^{-1}, MOND could explain satisfactorily the absence of a bar in this galaxy.

However, for NGC 3621, 5949 and 5963 the probability is less than 5% meaning that they require an abnormally large radial velocity dispersion to recover stability. We must stress that NGC 3621 and NGC 5949 are ideal systems to study their stability and can provide a stringent test to MOND because they are representative of pure-disc galaxies with no bars and MOND reproduces their high-resolution rotation curves fairly well, indicating that the distribution of mass in these galaxies is well determined in the MOND context.

NGC 5963 is a genuinely puzzling system in MOND; the fit to the rotation curve is poor and the disc is likely to be unstable to bar modes (unless σ_R at $1h_R$ is larger than ~ 70 km s^{-1}). It is unclear if a more realistic modelling, rather than using our oversimplifing assumptions (e.g. a constant $\Upsilon_\star$ across the galaxy, see §5.1), could bring this galaxy into agreement with observations.

Measurements of stellar velocity dispersions would be of enormous interest. The galaxies in our sample are suitable for measuring the stellar velocity dispersions because they have relatively high surface brightness (see Table 1). We need measurements of the velocity dispersions of old stars because they are the population that more contributes to the mass budget in the disc and thus the best tracer to infer the mass-weighted velocity dispersion, which is required to compute the Toomre parameter. Bottema & Gerritsen (1997) claimed that the velocity dispersions inferred in the B-band trace the old stellar population because a young population has far fewer absorption lines and they are located at the blue part of the optical spectrum (see also Bottema 1993). However, a contamination by young stars with low velocity dispersion would lead to an underestimate of the velocity dispersion. In fact, Fuchs (1999) estimated that in the solar neighbourhood, the velocity dispersion derived in the B-band is about 25% smaller than the mass-weighted velocity dispersion. For bluer galaxies, the B-band velocity dispersion could underestimate the mass-weighted velocity dispersion by a larger fraction. If galaxies were observed in the near V-band, as those used by Bershady et al. (2011), K-giants dominate the velocity dispersion signal (Aniyan et al. 2016). In the solar neigbourhood, an external observer that would fit the vertical velocity distribution with a single Gaussian would obtain a vertical velocity dispersion of 13.0 ± 0.1 km s^{-1}, which would translate to $\sigma_R = 22$ km s^{-1} (Aniyan et al. 2016), which is 50% smaller than the radial velocity dispersion of the old disc stars ($\simeq 44$ km s^{-1}, Binney & Tremaine 1987; Fuchs 1999).

It is worthwhile noting that, under MOND, a vertical velocity dispersion higher (by 30% on average) than derived from population-integrated line profiles, is also required to explain the thickness of 30 disc galaxies from the DiskMass survey (Angus et al. 2015; Milgrom 2015).

6 DISCUSSION AND CONCLUSIONS

We have analysed the dynamics of six late-type spiral galaxies in standard dark matter models and under MOND. The selected galaxies are bulgeless, show no evidence for strong bars, and they have high-quality measurements of the rotation curves, derived from two-dimensional velocity fields. In the sample, we have galaxies with relatively large internal accelerations ($\gtrsim a_0$) but cataloged as dark matter dominated galaxies (S05 and §4.1). Our main objective was to explore the capability of dark matter models and MOND to explain simultaneously the shape of the rotation curves and the level of gravitational stability of the discs with realistic stellar mass-to-light ratios. In particular, we examined the bar stability of these galaxies using the ENL and the PWC criteria. We summarize our main results below.

i) We found that for all the galaxies in our sample, one can adjust the dark halo parameters and the stellar mass-to-light ratio of the disc to match the rotation curves and the stability requirements.

ii) In the dark matter models, the bar stability criteria place upper limits on the value of $\Upsilon_\star$. We find that the stellar discs in two galaxies of our sample (NGC 3621 and NGC 6503) are submaximal, which means that the disc is not as massive as allowed by the rotation curve. In the case of NGC 6503, the upper limits derived with either ENL or PWC criteria are consistent with previous work.

iii) We have compared the upper limits on $\Upsilon_\star$ derived from stability arguments with population-synthesis values. We find that there are two galaxies, NGC 3621 and NGC 5949, where the upper $\Upsilon_\star$-value derived from stability analysis is a factor of $\sim 1.5 - 2$ lower than the population-synthesis value. Given that population-synthesis models have other sources of uncertainties besides the IMF (e.g., Conroy 2013), we conclude that dark matter models are consistent with observations for all the galaxies in our sample.

iv) There is some tension between the observed rotation curve and the MOND fit in three galaxies (NGC 4605, 5963 and 6503). These discrepancies cannot be explained by reasonable changes in the adopted value of a_0 or in the distances. For NGC 4605 and NGC 5963, MOND underpredicts the rotational speed at the outer parts of the observed rotation curve. In particular, in the case of NGC 5963, MOND predicts a gently declining rotation curve in the outer parts because the baryonic distribution is rather compact and the internal accelerations are larger than a_0. However, observations suggest that the rotation curve is slowly rising. It would be

worthwhile exploring whether the level of non-circular motions in these galaxies can affect the measured rotation curves.

v) In MOND, bar-stability requirements place lower limits to the stellar velocity dispersion. We find that the stellar discs in these galaxies should be dynamically hot, which may have observable consequences. In most of the galaxies (5 out of 6 galaxies), the required radial velocity dispersion of the stellar disc to be bar stable is significantly larger than the mean value observed in other galaxies with similar rotation velocity.

vi) Since the selected galaxies have central surface brightness as normal spiral galaxies, measurements of the stellar velocity dispersion until one radial scalelength should be feasible with mid-size telescopes.

vii) For one galaxy (NGC 6503), there is measurements of the stellar velocity dispersion. Taking the data at face value, the observed velocity dispersion is inconsistent with the value required to be bar stable in MOND.

viii) An alternative could be that the currently-available stellar velocity dispersions in external galaxies are not representative of the bulk of the stellar mass. This should be investigated further because it might have implications not only for MOND but also for Newtonian dark matter models.

Here we have focused on the global stability of the stellar disc in galaxies where the contribution of the gas to the mass budget is small. Low-mass gas-rich galaxies may be also interesting targets to check stability. Sánchez-Salcedo et al. (1999, 2014) found that gas-rich dwarf galaxies as IC 2574, NGC 1560 and Holmberg II, with measured H I velocity dispersions, are marginally stable in MOND and thus very responsive to perturbations. It remains a challenge for MOND to explain why these gas-rich galaxies have maintained a low rate of star formation.

ACKNOWLEDGEMENTS

We thank Carlo Nipoti for thoughtful comments and insightful suggestions on the manuscript. This work was partly supported by CONACyT project CB-165584. We acknowledge the usage of the HyperLeda database (http://leda.univ-lyon1.fr). The authors made use of the NASA/IPAC Extragalactic Database (NED) which is operated by the Jet Propulsion Laboratory, California Institute of Technology, under contract with the National Aeronautics and Space Administration, THINGS 'The H I Nearby Galaxy Survey' (Walter et al. 2008) and SDSS Data DR7. Funding for the SDSS and SDSS-II has been provided by the Alfred P. Sloan Foundation, the Participating Institutions, the National Science Foundation, the U.S. Department of Energy, the National Aeronautics and Space Administration, the Japanese Monbukagakusho, the Max Planck Society, and the Higher Education Funding Council for England. The SDSS Web Site is http://www.sdss.org/. This research has also made use of the NASA/IPAC Infrared Science Archive, which is operated by the Jet Propulsion Laboratory, California Institute of Technology, under contract with the National Aeronautics and Space Administration.

REFERENCES

Abazajian K. N., et al. 2009, ApJS, 182, 543
Adams J. J., Simon J. D., Fabricius M. H. et al. 2014, ApJ, 789, 63
Angus G. W., van der Heyden K. J., Famaey B., Gentile G., McGaugh S. S., de Blok W. J. G. 2012, MNRAS, 421, 2598
Angus G. W., Gentile G., Swaters R., Famaey B., Diaferio A., McGaugh S. S., van der Heyden K. J. 2015, MNRAS, 451, 3551
Aniyan S., Freeman K. C., Gerhard O. E., Arnaboldi M., Flynn C. 2016, MNRAS, 456, 1484
Athanassoula E. 1984, Phys. Rep., 114, 321
Athanassoula E. 2008, MNRAS, 390, L69
Athanassoula E., Bosma A., Papaioannou S. 1987, A&A, 179, 23
Athanassoula E., Sellwood J. A. 1986, MNRAS, 221, 213
Barnes J. E. 2016, MNRAS, 455, 1957
Barth A. J., Ho L. C., Sargent W. L. W. 2002, AJ, 124, 2607
Begeman K. G. 1987, Pn.D. thesis, Groningen State Univ.
Bekenstein J., & Milgrom M. 1984, ApJ, 286, 7
Bell E. F., & de Jong R. S. 2001, ApJ, 550, 212
Bershady M. A., Verheijen M. A. W., Westfall K. B., Andersen D. R., Swaters R. A., Martinsson T. 2010, ApJ, 716, 234
Bershady M. A., Martinsson T. P. K., Verheijen M. A. W., Westfall K. B., Andersen D. R., Swaters R. A. 2011, ApJ, 739, L47
Binney J., Tremaine S. 1987, Galactic Dynamics, Princeton Series in Astrophysics, Princeton University Press
Bolatto A. D., Simon J. D., Leroy A., Blitz L. 2002, ApJ, 565, 238
Bosma A., Athanassoula E., van der Hulst J. M. 1988, A&A, 198, 100
Bottema R. 1989, A&A, 221, 236
Bottema R. 1993, A&A, 275, 16
Bottema R. 2003, MNRAS, 344, 358
Bottema R., Gerritsen J. P. E. 1997, MNRAS, 290, 585
Bottema R., Pestaña J. L. G. 2015, MNRAS, 448, 2566
Bottema R., Pestaña J. L. G., Rothberg B., Sanders R. H. 2002, A&A, 393, 453
Brada R., Milgrom M. 1999, ApJ, 519, 590
Carignan C., Freeman K. C. 1988, ApJ, 332, L33
Conroy C. 2013, ARA&A, 51, 393
Côté S., Carignan C., Freeman K. C. 2000, AJ, 120, 3027
Curir A., Mazzei P., Murante P. 2006, A&A, 447, 453
Dale D. A. et al. 2009, ApJ, 703, 517
de Blok W. J. G., McGaugh S. S., Rubin V. C. 2001, AJ, 122, 2396
de Blok W. J. G., Walter F., Brinks E., Trachternach C., Oh S.-H., Kennicutt R. C. Jr. 2008, AJ, 136, 2648
D'Onghia E. 2015, ApJ, 808, L8
Efstathiou G., Lake G., Negroponte J. 1982, MNRAS, 199, 1069
Famaey B., & Binney J. 2005, MNRAS, 363, 603
Famaey B., Gentile G., Bruneton J.-P., Zhao H. 2007, PRD, 75, 063002
Famaey B., McGaugh S. 2012, Living Rev. Relativ., 15, 10
Freedman W. L. et al., 2001, ApJ, 553, 47
Forbes J. C., Krumholz M. R., Burkert A., Dekel A. 2014, MNRAS, 438, 1552
Fuchs B. 1999, in Merritt D., Sellwood J. A., Valluri M., eds, ASP Conf. Ser. Vol. 182, Galaxy Dynamics. Astron. Soc. Pac., San Francisco, p. 365
Fuchs B. 2001, A&A, 368, 107
Fuchs B. 2008, Astronomische Nachrichten, 329, 916
Fuchs B., von Linden S. 1998, MNRAS, 294, 513
Gentile G., Famaey B., & de Blok W. J. G. 2011, A&A, 527, 76
Ghosh S., Jog C. J. 2014, MNRAS, 439, 929
Ghosh S., Saini T. D., Jog C. J. 2016, MNRAS, 456, 943
Greisen E. W., Spekkens K., van Moorsel G. A. 2009, AJ, 137, 4718
James P. A. et al. 2004, A&A, 414, 23
Karachentsev I. D., & Sharina M. E. 1997, A&A, 324, 457

Kennicutt R. C. Jr. et al. 2003, PASP, 115, 928
Khoperskov A. V., Zasov A. V., Tyurina N. V. 2003, Astronomy Reports, 47, 357
Kormendy J., Drory N., Bender R., Cornell M. E. 2010, ApJ, 723, 54
Kregel M., van der Kruit P. C. 2005a, MNRAS, 358, 481
Kregel M., van der Kruit P. C., Freeman K. C. 2005b, MNRAS, 358, 503
Kuzio de Naray R., Arsenault C. A., Spekkens K., Sellwood J. A., McDonald M., Simon J. D., Teuben P. 2012, MNRAS, 427, 2523
Lira P., Johnson R. A., Lawrence A., Cid Fernandes R. 2007, MNRAS, 382, 1552
Lisker T., Fuchs B. 2009, A&A, 501, 429
Lynden-Bell D. 1979, MNRAS, 187, 101
Makarov D., Prugniel P., Terekhova N., Courtois H., Vauglin I. 2014, A&A, 570, 13
Makarova L. 1999, A&AS, 139, 491
Martinsson T. P. K., Verheijen M. A. W., Westfall K. B., Bershady M. A., Schechtman-Rook A., Andersen D. R., Swaters R. A. 2013, A&A, 557, 130
Mayer L., Wadsley J. 2004, MNRAS, 347, 277
Mayer L., Governato F., Colpi M., Moore B., Quinn T., Wadsley J., Stadel J., Lake G. 2001, ApJ, 559, 754
McGaugh S. S., de Blok W. J. G. 1998, ApJ, 499, 66
Mihos J. C., McGaugh S. S., de Blok W. J. G. 1997, ApJ, 477, L79
Milgrom M. 1983, ApJ, 270, 365
Milgrom M. 1986, ApJ, 302, 617
Milgrom M. 1989, ApJ, 338, 121
Milgrom M. 2010, MNRAS, 403, 886
Milgrom M. 2014, MNRAS, 437, 2531
Milgrom M. 2015, arXiv:1511.08087
Milgrom M., & Sanders R. H. 2007, ApJ, 658, L17
Milgrom M., & Sanders R. H. 2008, ApJ, 678, 131
Nipoti C., Ciotti L., Londrillo P. 2011, MNRAS, 414 3298
Persic M., Salucci P., Stel F. 1996, MNRAS, 281, 27
Pontzen A., Governato F. 2014, Nature, 506, 171
Puglielli D. 2011, ApJ, 739, 32
Puglielli D., Widrow L. W., Courteau S. 2010, ApJ, 715, 1152
Randriamampandry T. H., Carignan C. 2014, MNRAS, 439, 2132
Randriamampandry T. H., Combes F., Carignan C., Deg N. 2015, MNRAS, 454, 3743
Rodrigues D. C., de Oliveira P. L., Fabris J. C., Gentile G. 2014, MNRAS, 445, 3823
Romeo A. B., Falstad N. 2013, MNRAS, 433, 1389
Roshan M., Abbassi S. 2015, ApJ, 802, 9
Roskar R., Debattista V. P., Quinn T. R., Wadsley J. 2012, MNRAS, 426, 2089
Rubin V. C., Ford W. K. Jr., Thonnard N. 1980, ApJ, 238, 471
Saha K., Naab T. 2013, MNRAS, 434, 1287
Sánchez-Salcedo F. J., Hidalgo-Gámez A. M. 1999, A&A, 345, 36
Sánchez-Salcedo F. J., Hidalgo-Gámez A. M., Martínez-García, E. E. 2013, AJ, 145, 61
Sánchez-Salcedo F. J., Hidalgo-Gámez A. M., Martínez-García E. E. 2014, Revista Mexicana Astron. Astrofísica, 50, 225
Sanders R. H., McGaugh S. S. 2002, ARA&A, 40, 263
Sanders R. H., Noordermeer E. 2007, MNRAS, 379, 702
Sellwood J. A. 2016, ApJ, 819, 92
Sellwood J. A., Carlberg R. G. 1984, ApJ, 282, 61
Sellwood J. A., Evans N. W. 2001, ApJ, 546, 176
Sheth K. et al. 2010, PASP, 122, 1397
Simon J. D., Bolatto A. D., Leroy A., Blitz L. 2003, ApJ, 596, 957
Simon J. D., Bolatto A. D., Leroy A., Blitz L. 2005, ApJ, 621, 757
Slepian Z., Goodman J. 2012, MNRAS, 427, 839
Spano M., Marcelin M., Amram P., Carignan C., Epinat C., Hernandez O. 2008, MNRAS, 383, 297
Swaters R. A., Sanders R. H., McGaugh S. S. 2010, ApJ, 718, 380
Swaters R. A., Sancisi R., van Albada T. S., van der Hulst J. M. 2011, ApJ, 729, 118
Taylor V. A., Jansen R. A., Windhorst R. A., Odewahn S. C., Hibbard J. E. 2005, ApJ, 630, 784
Tiret O., Combes F. 2007, A&A, 464, 517
Toomre A. 1981, in Fall S. M., Lynden Bell D., eds, Structure and Evolution of Normal Galaxies. Cambridge Univ. Press, Cambridge, p. 111
Valenzuela O., Hernández-Toledo H., Cano M., Puerari I., Buta R., Pichardo B., Groess R. 2014, AJ, 147, 27
Walter F., Brinks E., de Blok W. J. G., Bigiel F., Kennicutt R. C., Thornley M., Leroy A. 2008, AJ, 136, 2563
Weijmans A.-M., Krajnovic D., van de Ven G., Oosterloo T. A., Morganti R., & de Zeeuw P. T. 2008, MNRAS, 379, 1343
Weinberg M. D., Katz N. 2002, ApJ, 580, 627
Yurin D., Springel V. 2015, MNRAS, 452, 2367
Zasov A. V., Khoperskov A. V., Tyurina N. V. 2004, Astronomy Letters, 30, 593

APPENDIX A: THE MOND X_M-PARAMETER IN TERMS OF NEWTONIAN VARIABLES: THE FICTIOUS DARK HALO

Consider a purely stellar disc in MOND. The stability parameters X_m depend on the rotation curve and its derivatives through κ, because conservation of angular momentum and differential rotation oppose to radial compressions in the disc. To go further, it is convenient to write κ^2 in terms of κ_N^2, which is defined as

$$\kappa_N^2 = R\frac{d\Omega_N^2}{dR} + 4\Omega_N^2, \tag{A1}$$

where $\Omega_N(R) \equiv v_{c,N}/R$. Thus, κ_N is the epicyclic frequency of the corresponding bare Newtonian disc (without the contribution of a dark halo). Using the identity $\Omega^2 = \Omega_N^2/\mu$, we obtain

$$\frac{d\Omega^2}{dR} = \frac{1}{\mu}\frac{d\Omega_N^2}{dR} - \frac{\Omega_N^2}{\mu^2}\frac{d\mu}{dR}, \tag{A2}$$

and

$$\kappa^2 = \frac{1}{\mu}\left(\kappa_N^2 - \frac{\gamma_N L}{1+L}\Omega_N^2\right), \tag{A3}$$

where

$$\gamma_N \equiv \frac{d\ln g_N}{d\ln R}. \tag{A4}$$

In the derivation of Equation (A3), we used the following identity: $\gamma_N = (1+L)\gamma_M$, where γ_M is the radial logarithmic derivative of g_M. Substituting Equation (A3) into Equation (9), we can write X_m as

$$X_m = \frac{\mu^+}{\mu}(1+L^+)^{1/2}\left(1 - \frac{L}{1+L}\left[\frac{\gamma_N}{3+\gamma_N}\right]\right)\frac{R\kappa_N^2}{2\pi G m\Sigma}. \tag{A5}$$

For a disc with $\mu^+ \simeq \mu$ and $L^+ \simeq L$, this expression can be simplified to

$$X_m \simeq \frac{1}{(1+L)^{1/2}}\left(1 + \frac{3L}{3+\gamma_N}\right)\frac{R\kappa_N^2}{2\pi G m\Sigma}. \tag{A6}$$

Thus, a galaxy under MOND has the same X_m-value than a Newtonian disc embedded in an inert dark halo with a mass fraction $f_d(R)$

$$f_d \equiv \frac{M_d(R)}{M_t(R)} \simeq (1+L)^{1/2}\left(1+\frac{3L}{3+\gamma_N}\right)^{-1}, \qquad \text{(A7)}$$

where $M_d(R)$ and $M_t(R)$ are, respectively, the mass of the disc and the total mass interior to R.

The smallest value of f_d occurs for galaxies in the deep MOND limit ($L \to 1$) and in regions where the Newtonian rotation curve of the disc decays in a Keplerian fashion ($\gamma_N = -2$). In that situation, $f_d \simeq 0.35$, which implies that the X_m-parameter in MOND is similar to add a dark halo 2 times as massive as the disc.

For galaxies with $x \simeq 1$ (hence $L \simeq 0.5$) and at intermediate radii, say $R \simeq 2.2h_R$ (so that $\gamma_N \simeq -1$), we have $f_d = 0.7$. This means that the value of X_m is similar to that in a Newtonian disc when it is immersed in a dark halo with a mass of only $\sim 0.4M_d$ within $2.2h_R$.

APPENDIX B: THE STABILITY PARAMETERS IN QUMOND

In the quasi-linear formulation of MOND (QUMOND, Milgrom 2010), the field equation is given by

$$\nabla^2\Phi = \boldsymbol{\nabla}\cdot\left[\nu(|\boldsymbol{\nabla}\Phi_N|/a_0)\boldsymbol{\nabla}\Phi_N\right], \qquad \text{(B1)}$$

where Φ_N is the Newtonian gravitational potential, which satisfies the Poisson equation

$$\nabla^2\Phi_N = 4\pi G\rho. \qquad \text{(B2)}$$

Here, $\nu(y)$ satisfies that $\nu \to 1$ when $y \gg 1$ (Newtonian limit) and $\nu \approx y^{-1/2}$ when $y \ll 1$.

In this Appendix, we are going to derive the change in the gravitational potential of a disc when we make a linear perturbation in the surface density. The procedure is standard and is frequently used to calculate the dispersion relation in discs (e.g., Binney & Tremaine 1987; Milgrom 1989; Roshan & Abbassi 2015). It is assumed that the disc is infinitesimally thin and use the tight winding approximation (WKB approximation).

The gravitational potential and forces in the disc are separated into the unperturbed part (denoted by a subscript 0) and the perturbations:

$$\Phi = \Phi_0 + \phi, \qquad \text{(B3)}$$

$$\Phi_N = \Phi_{N,0} + \phi_N, \qquad \text{(B4)}$$

$$\boldsymbol{g}_M = \boldsymbol{g}_{M,0} + \boldsymbol{q}_M, \qquad \text{(B5)}$$

and

$$\boldsymbol{g}_N = \boldsymbol{g}_{N,0} + \boldsymbol{q}_N. \qquad \text{(B6)}$$

Assuming that the perturbations are small, we linearize the QUMOND field equation (B1) and obtain

$$-\nabla^2\phi = -\nu_0\nabla^2\phi_N + \boldsymbol{q}_N\cdot\boldsymbol{\nabla}\nu_0 + \boldsymbol{\nabla}\left[\tilde{\nu}_0(\boldsymbol{q}_N\cdot\hat{\boldsymbol{e}}_0)\hat{\boldsymbol{e}}_0\right], \qquad \text{(B7)}$$

where $\tilde{\nu} \equiv y\nu'$ and $\hat{\boldsymbol{e}}_0 \equiv \boldsymbol{g}_{N,0}/g_{N,0}$ is the unit vector parallel to $\boldsymbol{g}_{N,0}$. Initially, we assume that the disc is axisymmetric. In that case, $\hat{\boldsymbol{e}}_0$ has only radial (e_R) and vertical (e_z) components.

We wish to calculate ϕ when the the perturbed surface density Σ_1 has the form of a tightly wound wave, that is

$$\Sigma_1 = \Sigma_\alpha \exp(ikR - i\omega t), \qquad \text{(B8)}$$

with $|kR| \gg 1$. This WKB approximation permits us to simplify calculations by neglecting terms proportional to $1/R$ compared with the terms proportional to k; thus the wave resembles locally a plane wave. As the perturbed quantities vary more quickly than the unperturbed variables, the gradients of the perturbed quantities are larger and so that we only retain derivatives of the perturbed quantities in Equation (B7). Outside the disc, $\nabla^2\phi_N = 0$, and the resultant differential equation for ϕ is

$$\nabla^2\phi = \tilde{\nu}_0\left[(e_z^2 - e_R^2)\frac{\partial^2\phi_N}{\partial z^2} + 2e_z e_R\frac{\partial^2\phi_N}{\partial R\partial z}\right]. \qquad \text{(B9)}$$

From the standard Newtonian analysis (e.g., Binney & Tremaine 1987), the perturbation on the Newtonian potential is given by

$$\phi_N = -\frac{2\pi G}{|k|}\Sigma_\alpha \exp(ikR - |kz| - i\omega t). \qquad \text{(B10)}$$

Once we know ϕ_N, we can compute its spatial derivatives and after substituting into Equation (B9), we derive a differential equation that obeys ϕ outside the disc:

$$\nabla^2\phi = 2\pi G\tilde{\nu}_0\mathcal{E}_0|k|\Sigma_\alpha \exp(ikR - |kz| - i\omega t), \qquad \text{(B11)}$$

where

$$\mathcal{E}_0 = 1 - 2e_z^2 - 2\mathrm{sgn}(k)ie_R|e_z|, \qquad \text{(B12)}$$

and sgn is the sign function. The solution of Equation (B11) that decays at large heights from the disc is given by

$$\phi = \phi_\alpha^{(1)}\exp(ikR - |kz| - i\omega t) \qquad \text{(B13)}$$
$$+2\pi G\tilde{\nu}_0\mathcal{E}_0\frac{|k|}{k_0^2 - k^2}\Sigma_\alpha \exp(ikR - |k_0 z| - i\omega t),$$

where $\phi_\alpha^{(1)}$ and k_0 are determined in the following by imposing the boundary conditions at $z = 0$.

Integrating Equation (B7) in a short cylinder whose flat faces are parallel to the disc and located at $z = \pm h$, with $h \to 0$, we find that

$$\left.\frac{\partial\phi}{\partial z}\right|_{z=0^+} = \nu_0^+\left.\frac{\partial\phi_N}{\partial z}\right|_{0^+} + \tilde{\nu}_0^+\left(\left.\frac{\partial\phi_N}{\partial z}\right|_{0^+} e_z^+ + \left.\frac{\partial\phi_N}{\partial R}\right|_{0^+} e_R\right)e_z^+, \qquad \text{(B14)}$$

where ν_0^+, $\tilde{\nu}_0^+$ and e_z^+ are the values of ν_0, $\tilde{\nu}_0$ and e_z just above the disc. Substituting the $R-$ and $z-$derivatives of ϕ_N into Equation (B14), we get

$$\left.\frac{\partial\phi}{\partial z}\right|_{z=0^+} = 2\pi G\Sigma_\alpha \exp(i[kR - \omega t]) \qquad \text{(B15)}$$
$$[\nu_0^+ + \tilde{\nu}_0^+(e_z^+)^2 + \tilde{\nu}_0^+\mathrm{sgn}(k)ie_R|e_z^+|].$$

By equating Equation (B16) with the z-derivative of Equation (B14), we obtain

$$\frac{|kk_0|}{k_0^2 - k^2} = \frac{1}{2}, \qquad \text{(B16)}$$

which implies that $k_0 = \pm(1+\sqrt{2})k$ (note that the choice of the sign of k_0 is physically irrelevant). We also obtain that

$$-|k|\phi_\alpha^{(1)} - \pi G\tilde{\nu}_0^+\Sigma_\alpha = 2\pi\nu_0^+ G\Sigma_\alpha, \qquad \text{(B17)}$$

implying

$$\phi_\alpha^{(1)} = -\frac{2\pi(\nu_0^+ + \tilde{\nu}_0^+/2)G\Sigma_\alpha}{|k|}. \quad \text{(B18)}$$

Combining Eqs. (B14) and (B18) and using that $k_0 = \pm(1+\sqrt{2})k$, we finally find the perturbation on the gravitational potential in the plane of the disc:

$$\phi(R,0) = -\frac{2\pi\chi_Q G\Sigma_1}{|k|}, \quad \text{(B19)}$$

with

$$\chi_Q = \nu_0^+ + \frac{\tilde{\nu}_0^+}{2}\left(1 - \frac{\mathcal{E}_0^+}{1+\sqrt{2}}\right). \quad \text{(B20)}$$

Therefore, the linear perturbation on the QUMOND potential, the QUMOND Toomre criteria and the X_m-parameters can be obtained by replacing G for $\chi_Q G$ in the respective Newtonian formulae

$$Q = \frac{\sigma_R \kappa}{\pi\chi_Q G\Sigma}, \quad \text{(B21)}$$

$$X_m = \frac{R\kappa^2}{2\pi m \chi_Q G\Sigma}. \quad \text{(B22)}$$

In a thin rotating disc, the z-component of the acceleration is much smaller than the local radial acceleration and hence $\mathcal{E}_0^+ = 1$. In that case

$$\chi_Q = \nu_0^+ + \left(1 - \frac{1}{\sqrt{2}}\right)\tilde{\nu}_0^+ = \nu_0^+\left(1 + \left[1 - \frac{1}{\sqrt{2}}\right]\mathcal{L}_0^+\right), \quad \text{(B23)}$$

where $\mathcal{L} = y\nu'/\nu$.

In the Newtonian limit, $\nu_0^+ = 1$ and $\mathcal{L}_0 = 0$. Consequently $\chi = 1$ and the classical Newtonian case is recovered. In the deep MOND regime, $\mathcal{L}_0 = -1/2$, and then

$$\chi_Q = \frac{\nu_0^+}{2}\left(1 + \frac{1}{\sqrt{2}}\right). \quad \text{(B24)}$$

In order to compare QUMOND with the non-linear Poisson formulation regarding the degree of stability, it is convenient to write down χ_Q in terms of μ^+ and L^+ using the relations

$$\nu(y) = \frac{1}{\mu(x)}, \quad \text{(B25)}$$

and

$$\mathcal{L} = -\frac{L}{1+L}. \quad \text{(B26)}$$

We obtain

$$\frac{\chi_Q}{\chi_{nl}} = \frac{1}{(1+L^+)^{1/2}}\left(1 + \frac{L^+}{\sqrt{2}}\right). \quad \text{(B27)}$$

It holds that $\chi_Q \geq \chi_{nl}$, suggesting that self-gravitating discs are more stable in the non-linear Poisson formulation than they are in QUMOND. For discs with $L^+ \simeq 0.5$, as those considered in this work, $\chi_Q/\chi_{nl} \simeq 1.1$.

APPENDIX C: MODEL INFERENCE USING A BAYESIAN APPROACH

Bayesian inference relies on the concept of conditional probability to revise one's knowledge. Prior to the collection of sample data one had some (perhaps vague) information on the parameter of interest θ. This initial uncertainty is formally modelled via a *prior distribution* for the parameter θ. In our case the parameter of interest is $\Upsilon_\star$. Then using Bayes Theorem we can combine the model density of the observed data with the prior density to get the *posterior density*, that is, the conditional density of θ given the data. Until further data is available, this posterior distribution of θ is the only relevant information as far as is concerned.

Some notation is required to describe the Bayesian perspective. Let us denote the prior distribution by $\pi(\theta)$. Let n be the number of observations for a given galaxy. The model for the observed data $\mathbf{y} = (y_1, y_2, \ldots, y_n)$ is expressed by the likelihood function $\mathcal{L}(\theta) = f(\mathbf{y}|\theta)$. The joint distribution of the data and the parameter of interest is given by:

$$f(\mathbf{y}, \theta) = f(\mathbf{y}|\theta)\pi(\theta) = \mathcal{L}(\theta)\pi(\theta).$$

One can update the knowledge on θ by computing the conditional distribution of θ given the information in the sample $\mathbf{y}$. This is done via Bayes Theorem that states that the *posterior distribution* of θ is given by

$$\pi(\theta|\mathbf{y}) = \frac{f(\mathbf{y}|\theta)\pi(\theta)}{\int f(\mathbf{y}|\theta)\pi(\theta)d\theta}. \quad \text{(C1)}$$

There is a simulation method called Markov Chain Monte Carlo that generates a sequence of values of θ, say $\{\theta_i\}_{i=1}^{MC}$, that has a distribution equal to (C1). This method has the advantage that avoids the need to compute the integral in the denominator of the right-hand-side of Equation (C1). The method just requires the specification of the likelihood function and the prior density. The value of MC is usually huge, say $100,000$.

For this Bayesian approach we assume the simplest prior distribution for the unknown parameter θ, that is, the Jeffrey's prior (also known as uniform or flat prior). The upper limit for this distribution was obtained using stability arguments to provide upper limits on the surface density of stellar disks, as mentioned in the introduction. For the likelihood function we assume that the discrepancies between the rotation velocities and the model in question have a normal distribution. This can be expressed as

$$f(\mathbf{y}|\theta) \propto \exp\left(-\frac{1}{2}\sum_{i=1}^{n}\left[\frac{y_i - \mu(x_i,\theta)}{\sigma_i}\right]^2\right),$$

where y_i is the observed rotation velocity at the corresponding radius x_i, $\mu(x_i,\theta)$ is a nonlinear specification that depends on the astro-dynamics of each galaxy and σ_i^2 is the measurement error.

Once we obtain a sequence of values $\{\theta_i\}_{i=1}^{MC}$ from the posterior distribution $\pi(\theta|\mathbf{y})$ we use them to make inferences on a nonlinear, non-monotonic transformation $g(\theta)$ by computing the sequence $\{g(\theta_i)\}_{i=1}^{MC}$. From this we calculate a point estimator using the average, $\frac{1}{MC}\sum_{i=1}^{MC} g(\theta_i)$, or the median. In order to obtain a $(1-\alpha)\%$ interval that reflects the uncertainty in the estimation we used the percentiles of $\frac{\alpha}{2}\%$ and $(1-\frac{\alpha}{2})\%$ of this sequence to obtain a posterior credibility interval for $g(\theta)$.

For example, $X_2(R, \Upsilon_\star)$ is a highly nonlinear function of $\Upsilon_\star$. Using the above method we were able to obtain the bands in Figure 9. Also $\langle X_2 \rangle$ is the average of a highly nonlinear function of $\Upsilon_\star$. Using the above method we were able to obtain posterior credibility intervals for its value, which are given in Table 3.

It is important to stress the relevance of using the Bayesian approach for the models studied in this paper. The models under consideration are highly non-linear functions of the parameter of interest. In statistics this is usually treated using approximate methods that assume a large sample, that is a value of n in the order of hundreds. This is not the case in our samples; hence those approximations are expected to produce inconsistent results in these

models. For example, using the large sample methods, the bands for $X_2(R, \Upsilon_\star)$ or the interval for $\langle X_2 \rangle$ could very well include negative values.